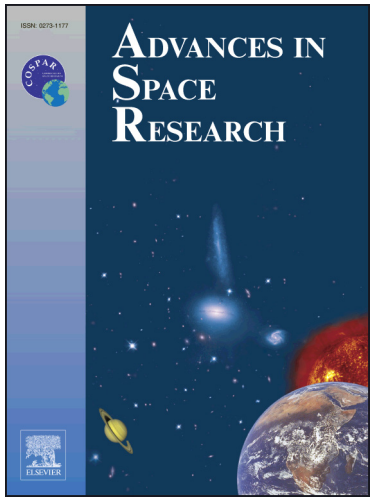

MUSE - Mission to the Uranian System: Unveiling the evolution and formation of ice giants

Tatiana Bocanegra-Bahamón, Colm Bracken, Marc Costa Sitjà, Dominic Dirkx, Ingo Gerth, Kostas Konstantinidis, Christos Labrianidis, Matthieu Laneuville, Armin Luntzer, Jane L. MacArthur, Andrea Maier, Achim Morschhauser, Tom A. Nordheim, Renaud Sallantin, Reinhard Tlustos

PII: S0273-1177(15)00089-7
DOI: http://dx.doi.org/10.1016/j.asr.2015.01.037
Reference: JASR 12126

To appear in: *Advances in Space Research*

Received Date: 14 February 2014
Revised Date: 15 November 2014
Accepted Date: 29 January 2015

Please cite this article as: Bocanegra-Bahamón, T., Bracken, C., Sitjà, M.C., Dirkx, D., Gerth, I., Konstantinidis, K., Labrianidis, C., Laneuville, M., Luntzer, A., MacArthur, J.L., Maier, A., Morschhauser, A., Nordheim, T.A., Sallantin, R., Tlustos, R., MUSE - Mission to the Uranian System: Unveiling the evolution and formation of ice giants, *Advances in Space Research* (2015), doi: http://dx.doi.org/10.1016/j.asr.2015.01.037

MUSE - Mission to the Uranian System: Unveiling the evolution and formation of ice giants

Tatiana Bocanegra-Bahamón

Department of Astrodynamics and Space Missions, Delft University of Technology, 2629 HS Delft, The Netherlands.

Joint Institute for VLBI in Europe, P.O. Box 2, 7990 AA Dwingeloo, The Netherlands.

Shanghai Astronomical Observatory, 80 Nandan Road, Shanghai 200030, China.

Colm Bracken

National University of Ireland. Maynooth, Co. Kildare, Ireland.

Marc Costa Sitjà

INSA/ESA, European Space Astronomy Centre (ESAC), P.O. Box 78, E-28691 Villanueva de la Cañada, Madrid, Spain.

Dominic Dirkx

Department of Astrodynamics and Space Missions, Delft University of Technology, 2629 HS Delft, The Netherlands.

Ingo Gerth

Department of Astrodynamics and Space Missions, Delft University of Technology, 2629 HS Delft, The Netherlands.

Kostas Konstantinidis

Universitaet der Bundeswehr Muenchen, Werner-Heisenberg-Weg 39, 85577 Neubiberg, Germany.

Christos Labrianidis

Tesat-Spacecom GmbH & Co., Gerberstrasse 49, D-71522 Backnang, Germany.

Matthieu Laneuville

Institut de Physique du Globe de Paris, Sorbonne Paris Cité, Univ. Paris Diderot, 5 rue Thomas Mann, 75205 Paris Cedex 13, France.

Armin Luntzer

Department of Astrophysics, University of Vienna, Universitätsring 1, 1010 Vienna, Austria.

Jane L. MacArthur

Department of Physics and Astronomy, Centre for Planetary Science at UCL/Birkbeck, University College London, Gower Street, London, WC1E 6BT, UK.

Andrea Maier

Space Research Institute, Austrian Academy of Sciences, Schmiedlstrasse 6, 8042 Graz, Austria.

Achim Morschhauser

German Aerospace Center (DLR), Planetary Physics, Rutherfordstrasse 2, 10997 Berlin, Germany

Tom A. Nordheim

Centre for Planetary Science at UCL/Birkbeck, University College London, Gower Street, London, WC1E 6BT, UK.

Mullard Space Science Laboratory, University College London, Holmbury St Mary, Dorking, RH5 6NT, UK.

Renaud Sallantin

*Corresponding author

Email address: t.m.bocanegrabahamon@tudelft.nl (Tatiana Bocanegra-Bahamón)

CNES, University of Toulouse, 2 Rue Charles Camichel, Toulouse, France

Reinhard Tlustos

Department of Astrophysics, University of Vienna, Universitätsring 1, 1010 Vienna, Austria.

Abstract

The planet Uranus, one of the two ice giants in the Solar System, has only been visited once by the Voyager 2 spacecraft in 1986. Ice giants represent a fundamental class of planets, and many known exoplanets fall within this category. Therefore, a dedicated mission to an ice giant is crucial to improve the understanding of the formation, evolution and current characteristics of such planets in order to extend the knowledge of both the Solar System and exoplanetary systems.

In the study at hand, the rationale, selection, and conceptual design for a mission to investigate the Uranian system, as an archetype for ice giants, is presented. A structured analysis of science questions relating to the Uranian system is performed, categorized by the themes atmosphere, interior, moons and rings, and magnetosphere. In each theme, science questions are defined, with their relative importance in the theme quantified. Additionally, top-level weights for each theme are defined, with atmosphere and interior weighted the strongest, as they are more related to both exoplanetary systems and the Uranian system, than the other two themes (which are more specific for the planet itself). Several top level mission architecture aspects have been defined, from which the most promising concepts were generated using heuristic methods. A trade-off analysis of these concepts is presented, separately, for engineering aspects, such as cost, complexity, and risk, and for science aspects. The science score for each mission is generated from the capability of each mission concept to answer the science questions. The trade-off results in terms of relative science and engineering weight are presented, and competitive mission concepts are analyzed based on the preferred mission type.

A mission design point for a typical flagship science mission is selected from the trade space. It consists of a Uranus orbiter with a dry mass of 2073 kg including 402 kg of payload and a Uranus entry probe, which is to perform measurements down 100 bar atmospheric pressure. The orbiter science phase will consist of a Uranus orbit phase of approximately 2 years in a highly elliptical orbit, during which 36 Uranus orbits are performed. Subsequently, a moon phase is performed, during which the periapsis will be raised in five steps, facilitating 9 flybys of each of Uranus' major moons. A preliminary vehicle design is presented, seeking the best compromise between the design drivers, which basically derive from the large distance between Uranus and the Earth (*e. g.*, high thermal load during Venus flyby, low thermal load during Uranus science phase, low data-rate during Uranus science phase, the need of radioisotope power source, etc).

This paper is the result of a study carried out during the Alpbach Summer School 2012 "Exploration of the icy planets and their systems" and a one-week follow-up meeting in Graz, Austria. The results of this study show that a flagship ESA L-class mission - consisting of an orbiter with a single atmospheric entry probe and flybys of the main satellites - would be able to address the set of science questions which are identified in the study at hand as the most essential for the understanding of Uranus and its system. The spacecraft, as currently designed, could be launched with an Ariane 5, in 2026, arriving at Uranus in 2044, and operating until 2050. The development of a radioactive power source is the main requirement for feasibility for this mission.

Keywords: Uranus; Ice Giants; Orbiter; Probe; Moon Tour

1. Introduction

Out of the four giant planets in the Solar System, only the Jovian and Saturnian systems have been investigated by orbiting robotic probes (*e.g.*, Johnson et al. (1992); Matson et al. (2003)). In-system investigation of the ice giants have so far been limited to the flyby of both Uranus and Neptune by Voyager 2 during its grand tour in 1986 (Stone & Miner, 1986). Since then, scientific progress has been made with ground-based observations (*e.g.*, Sromovsky (2000)) and telescopic surveys from Earth orbit (*e.g.*, Karkoschka (2001)). Due to the physical limitations of such observations, stemming from the long distance to these planets, the limited variation in observation geometries, and the lack of in-situ and close-up measurements, many of the ice giants' often peculiar properties are poorly constrained, and its role in the evolution of the Solar System is not well understood (*e.g.*, Levison (2001)).

Despite the high potential for scientific return, no dedicated orbital mission is planned to explore either of the ice giants and their systems. For example, a mission to Uranus could help answer why its rotational axis lies almost in the ecliptic, why its magnetic field axis is considerably inclined with respect to the planet's rotational axis (Ness et al., 1986), and why the ice giants are located at such large distances from the Sun, while most recent models predict a much smaller semi-major axis (Levison, 2001; Stevenson, 2004). Also, many of the extrasolar planets discovered to date have similar masses as those of the Solar System's ice giants. As a result, in situ investigation of ice giants, which remain the least understood planets in our Solar System, could provide a "ground truth" for interpretation of exoplanet observations and aid future development of ice giant formation and evolution theories in general (Schneider et al., 2011). For these reasons, an orbiter, capable of in-situ observations of the Uranian system with a dedicated instrument suite would add substantially to scientific knowledge of both, the Solar system and planetary systems in general.

There have been several recent mission studies for ice giant missions, such as those by Turrini et al. (2013), Arridge et al. (2011) and Hubbard (2010), which have taken part in surveys for future large-size mission concepts, such as, the European Space Agency(ESA) Call for Science Themes for L2 and L3 Missions (ESA, 2013), and the National Research Council (NRC) Planetary Science Decadal Survey 2013-2022 (Squyres et al., 2011). The selection panels of both surveys have recognized the importance of a dedicated ice giant mission.

In this paper, the need for a mission to Uranus will be explained by discussing the scientific case, providing an extensive investigation of the scientific and engineering trade-space, and demonstrating the technical feasibility of such a mission, by means of a point-design mission study. A complete envelope of science questions and technical architectures has been established, and consolidated into several top-level design options. Based on the engineering constaints, science goals, their relative importance, and the capability of each mission concept to meet these goals, the best candidate has been selected in a systematic trade-off, with the results presented as a function of relative science and engineering criteria weights. The selected mission concept for the Mission to Uranian System Explorer (MUSE), chosen from a point-design of a typical flagship-class science mission, consists of a single Uranus orbiter and a Uranus atmospheric entry probe.

MUSE's system design consists of a 4240 kg wet mass spacecraft including 90 kg of scientific payload, as well as a 312 kg Uranus entry probe. It is to be launched by an Ariane 5 in 2026, arriving at Uranus in 2044. Following a Uranus orbit phase of 2 years, the spacecraft is to perform flybys of Uranus five major moons. The primary mission end is planned for 2050. The development of a radioactive power source is the main requirement for attaining technical feasibility. Studies for this are ongoing in Europe, where the use of ^{241}Am as a heat source for generating electricity is being developed (O'Brien et al., 2008). Arridge et al. (2011) have expressed that although being a key enabling technology, this development is feasible.

This paper is the result of a study conducted during the Alpbach Summer School 2012 "Exploration of the icy planets and their systems" and a one-week follow-up meeting in Graz, Austria. The paper is structured as follows: current knowledge and open questions about the Uranian system are summarized in Section 2. Based on this, a science case is defined in Section 3. This allows a detailed mission architecture trade, which is presented in Section 4. Subsequently, Section 5 presents the mission analysis aspects of the system, and the resulting space segment is discussed in Section 6, highlighting the spacecraft design. Some programmatic implications are discussed in Section 7, with conclusions and recommendations in Section 8.

2. Current Knowledge of the Uranian System

The first recorded sighting of Uranus was reported by John Flamsteed in 1690, although he classified it as a star, 34 Tauri (Airy, 1847). Further observations were made by others, but William Herschel was credited with the discovery of the planet in 1781, with universal acknowledgement in 1783 (Airy, 1847). It was observed to be 14.5 times more massive than Earth, with one orbit taking 84 Earth years to complete.

Table 1: Basic facts about the Uranian system (Stone & Miner, 1986).

Aphelion	20.1 AU
Perihelion	18.4 AU
Orbital period	84.3 yr
Number of known satellites	27 (5 larger moons)
Orbital speed	6.8 km/s
Axial tilt	97.8°
Magnetic field tilt	59°
Equatorial radius	25.559 ± 4 km
Polar radius	24.973 ± 20 km

In order to better understand the origin and evolution of the Uranian system, four particular science areas have been defined:

- **Atmosphere:** The atmosphere, being the outermost and most accessible layer of the planet, can provide information on the chemistry, dynamics, and heat transport mechanisms of Uranus' interior. As it is far out in the Solar System, cosmic ray chemistry becomes important.
- **Interior:** Understanding the interior structure and dynamics is essential to understand how Uranus formed and evolved. Its exact composition, particularly in regard to heavy elements, is not known and it is still unclear whether Uranus possesses a rocky core.
- **Magnetosphere:** Due to the magnetic dipole tilt of nearly 60° with respect to the rotation axis, the Uranian magnetosphere has a unique and highly dynamical configuration, which offers the possibility to test existing theories in a complex and highly variable magnetosphere.
- **Moons and Rings:** Uranus possesses a system of moons and rings in its equatorial plane, which are believed to interact dynamically and chemically, with some moons showing evidence of interesting past geologic activity. However, details are largely unknown.

With respect to the mission objectives each of these science areas were prioritized. The atmosphere and interior were found to be the most important subjects, as the presence of an inner core and the detailed elemental abundances and isotopic ratios hold information on the physical and chemical conditions during formation and subsequent evolution. The dynamics of the atmosphere, as well as for instance the presence of non-equilibrium species, will give insights into heat transport mechanisms and evolution of the planet.

In the following sections, Uranus is described in a broader context, followed by a more detailed overview of the current knowledge and main problems in each of the four proposed areas.

2.1. Uranus: key to understanding the formation and evolution of the Solar System

The Uranian system, consisting of the planet itself, its moons, and its rings, holds many clues to the formation and evolution of the Solar System. Similar in mass and density to Neptune, the relative amounts of heavy elements such as oxygen, carbon, nitrogen and sulfur are significantly lower than for Jupiter and Saturn (Guillot & Gautier, 2007). As these heavy elements are mainly present in the form of water, methane, and ammonia at shallow depths, Uranus and Neptune are referred to as ice giants.

The presence of the ice giants poses some challenges to standard theories of Solar System formation (*e. g.*, Levison (2001); Stevenson (2004)). In principle, there are two competing models, namely the core accretion and the disk instability model, both of which have been adapted to explain the formation of the ice giants. According to the disk instability model (Boss, 1997; Mayer, 2002), planets form due to gravitational collapse in the accretion disk, similar to the formation of stars. In this model, it is assumed that the ice giants have lost most of their gaseous envelope due to strong extreme ultraviolet radiation of neighboring, young stars (Boss, 2002). The core

accretion model (Mizuno, 1980), on the other hand, assumes gravitational growth of solid, rocky particles, which will accrete a massive gaseous envelope when reaching a critical mass of around 5-30 Earth masses (*e. g.*, Pollack (1996); Hubickyj et al. (2005)). In this case, Uranus and Neptune could not have formed within the timescale of the existence of the accretion disk, when enough dust particles were still present. Planetary migration has been suggested to resolve this problem (Alibert et al., 2005). As both of these models have difficulties in predicting the existence of Uranus and Neptune, it is essential to study Uranus in more detail. This will help to constrain theories on planet formation and lead to a better understanding of how the Solar System formed.

Furthermore, the thermal evolution of Uranus is not well understood. While homogeneous evolution models correctly predict today's luminosity for Jupiter and Neptune, Saturn's is predicted to be lower and Uranus' to be higher than observed (Fortney et al., 2011). In the case of Uranus, it has been suggested that this might be due to sequestration and inefficient convection in the planet's interior (Lunine, 1993).

With the detection of extrasolar planets, our understanding of the Solar System is put into a broader context. A great variety of configurations have been detected, such as fast orbiting planets close to the host star, super-Earths, or mini-Jupiters, which resemble the ice giants in the Solar System. The discovery of these planets challenges current theories of Solar System formation (Bodenheimer & Lin, 2002), and a precise understanding of the processes in the Solar System is necessary in order to understand the formation and diversity in extrasolar planetary systems.

2.2. Atmosphere

The atmosphere, being the interface between the interior and exterior, is most accessible to (in situ) remote sensing and contains valuable information on interior dynamics, heat transport, chemical composition and the interactions of the planet, and its space environment. The Uranian atmosphere consists of the stratosphere, where temperatures rise with altitude due to absorption of solar radiation in different wavelengths, the convective lower troposphere, the radiative upper troposphere, as well as the ionosphere and exosphere.

As the Uranian troposphere is much colder than those of Jupiter and Saturn, ground-based thermal-infrared (IR) spectroscopy is complicated due to the low IR fluxes and due to the fact that little is known about the composition of the Uranian atmosphere. The atmosphere of Uranus consists mainly of hydrogen and helium, with a ratio of 1 : 7 at pressures around 1 bar (Conrath et al., 1987; Baines, 1995). However, the hydrogen-helium envelope, usually referred to as the atmosphere, is a rather thin shell, accounting for only 20% of the radius (Irwin, 2009). Methane is by far the third-most abundant element in the atmosphere with a vertical mixing ratio of around 1-2% (Lindal et al., 1987; Baines, 1995; Sromovsky & Fry, 2008).

Due to the lower tropospheric temperatures, clouds will condensate at lower levels as compared to Jupiter and Saturn. Methane clouds have been detected to form at around 1.5 bar (Baines & Bergstralh, 1986; Baines, 1995), as predicted by models. The presence of different cloud layers has important implications on atmospheric thermal structure. For example, observed microwave spectra suggest that the atmospheric temperature profile becomes isothermal at depth (De Pater et al., 1989), but the observed spectrum may also be explained by a deep, optically thick cloud layer, such as the expected water cloud layer (Irwin, 2009). Also, water vapor abundances down to 50 bar were found to be sub-solar, indicating the presence of a deep water cloud layer, which presumably exists between 100 and 1000 bar, depending on the exact H_2O/H_2 ratio and temperature profile (Irwin, 2009).

For Uranus, the observed energy balance, i.e., the ratio of absorbed and emitted energy is 1.06, much lower than thermal evolution models predict. Therefore, it would be expected that circulation in the atmosphere is sluggish. However, temperature differences in the 0.5 to 1 bar pressure levels as measured by Voyager 2 were much smaller than expected during south polar solstice (Flasar et al., 1987; Hanel et al., 1986). The energy source of such a thermal redistribution is still unclear.

2.3. Interior

As the internal structure of Uranus cannot be observed directly, theoretical models of the internal composition, temperature and pressure are used. These models are fit to the observable data such as the planet's bulk density and moment of inertia. Interior structure models rely mainly on equations describing hydrostatic equilibrium, conservation of mass and energy, and assume a simplified planetary shape (Guillot, 2005). As the interior structure gets more complex, other observables have to be used as constraints, such as heat flow, magnetic field, zonal wind structure, or tidal evolution.

The standard model of Uranus' structure suggests that the innermost region of the planet consists of rock (magnesium, silicon, and iron), the intermediate region consists of ice (water, methane, and ammonia), and the outermost region consists of gas (hydrogen and helium) (Podolak et al., 1991). It should be noted that "rock", "ice", and "gas" do not refer to the phase of the material. Due to high temperature and pressure in the interior

it is expected that all components behave as liquids. The intermediate region accounts for ∼85% of the total mass of Uranus. The innermost and outermost regions contribute less than 3% and 15%, respectively (Miner, 1990). Hubbard & Marley (1989) summarize interior models of Uranus published after the Voyager 2 flyby. These models all conclude that a major separation of Uranus into its individual rock and ice components has not taken place. However, there seems to be a rapid increase in the heavy-element composition at pressures greater than ∼100 kbar.

Nevertheless, deducing chemical composition from interior structure modeling is non-trivial, as a variety of mixtures can give the same pressure-density relation (Hubbard & Marley, 1989). In addition, recent revision in the rotation period and flattening of Uranus has shown how dependent the results are on such parameters (Nettelmann et al., 2013). While the bulk composition is in agreement with previous models, they predict different mass fractions in the atmosphere. As a consequence, Uranus and Neptune may actually have different internal structures.

In summary, the density distribution of Uranus is well known from Voyager 2 data (Guillot & Gautier, 2007). Various models, however, show differences with respect to the non-unique composition of the postulated three regions of Uranus' interior (Podolak et al., 1991). Better accuracy of measurements of Uranus' gravity field, rotational rate and atmospheric composition will therefore help to build better interior models and thus shed light on exoplanet observations and Solar System formation.

2.4. Moons and Rings

Uranus is surrounded by a complex and diverse system of moons, which interact dynamically with the ring system, likely exchanging matter (French et al., 1991). To date 27 Uranian moons have been discovered (Bond, 2012), five of which have a radius greater than 100 km. The ring system consists of 13 known rings. Most of the material is confined to the nine innermost, while the outermost, μ and ν, were discovered only recently using the Hubble Space Telescope (HST) due to their much lower optical thicknesses (Showalter, 2006).

Classes of moons can be distinguished from their orbital characteristics. Regular ones have a mostly circular orbit and orbit in a prograde direction, while irregular ones generally have a highly eccentric, inclined and retrograde orbit. Regular moons are thought to have formed in the Uranian system at the same time as Uranus, whereas irregular moons were probably captured later (Guillot & Gautier, 2007). All of them orbit close to Uranus' equatorial plane, which is non trivial to explain, since Uranus' rotation axis is tilted by 97°. The best scenario to date involves a giant impact, from which the regular moons were formed by accretion of the post-impact disk (Slattery et al., 1992). New information on the moons will help to add constraints on this model. Another hypothesis is that Uranus' inclination occurred adiabatically on a long timescale, and therefore the moon system was rotated at the same time (Canup & Ward, 2000).

Voyager 2 imaging data revealed interesting features on the surface of all major satellites, leading to the conclusion that they are most likely differentiated (Miner, 1990). Of these, Miranda shows extensive surface processes, thought to have been driven by tidal heating caused by a past orbital resonance with Umbriel. Ariel, on the other hand, shows the most recent signs of geological activity with a relative lack of large craters, suggesting that Ariel has been resurfaced in its history, making these moons the most interesting geological target in the Uranian system. Further, some authors suggest that subsurface oceans might exist in Titania and Oberon (Hussmann et al., 2006; England, 2003). Due to its particular flyby trajectory, Voyager 2 imaged only the southern hemispheres of the satellites. New imaging data will therefore provide important additional information to understand the origin and evolution of these moons.

The ring system of Uranus was discovered during a stellar occultation by Uranus in 1977. Voyager 2 imagery provided the first two-dimensional information about the rings, including the discovery of two additional rings in 1986 (Smith et al., 1986). The ring system lies within 2 Uranus radii and the width of the rings range between 1 and 10 km. Although, the two rings discovered recently by the HST (Showalter, 2006), μ and ν, are much wider (∼15000 km and ∼4000 km, respectively). The particles in the nine optically thick rings are approximately 10 cm to 10 m in size. They are extremely dark, which suggests they are carbon rich. The outermost μ ring is blue, which indicates submicrometer sized particles. Most, if not all of the rings, are not primordial. Their very dynamic nature can help to understand the history of the Uranian system, and the interactions between Uranus, its moons, and its rings.

To date, the mechanism which confines the eight inner rings is not known (Smith et al., 1986). Orbital simulations of eight densely packed moons between the inner ring region and the major moons, known as the Portia group, show that they are dynamically unstable on a 1 to 100 Ma timescale (Duncan & Lissauer, 1997). The recent discovery of two new moons and two new rings (Showalter, 2006), in addition to the fact that the largest moons also show orbital changes within decades, all contribute to the idea that the Uranian ring-moon

system is a rapidly and chaotically evolving system, in which stochastic processes are more important than previously thought. Overall, Voyager 2 merely made a snapshot of that system, and a better model of its underlying dynamics will help to understand its evolution (Miner, 1990).

2.5. Magnetosphere

Uranus possesses a strong intrinsic magnetic field, with a dipole moment roughly comparable to those of Saturn and Neptune. It exhibits strong quadrupole and higher-order moments, and its dipole is highly offset from the center of the planet (Ness et al., 1986). In combination with the highly inclined rotational axis of Uranus, this produces a unique magnetospheric configuration, where one of the magnetic poles is oriented almost directly towards the incoming solar wind flow during equinox. At solstice, the magnetotail takes on a twisted configuration not known to exist elsewhere in the Solar System (Tóth et al., 2004).

During the Voyager 2 flyby, Uranus was at solstice and the magnetic rotation axis was nearly side-on to the solar wind. This magnetospheric configuration results in a decoupling of solar-wind driven convection and magnetospheric co-rotation, allowing solar-wind convection to penetrate deep into the magnetosphere (Selesnick & Richardson, 1986; Vasyliunas, 1986). However, at other configurations of the Uranian magnetosphere (*e. g.*, equinox, when the magnetic pole faces the solar wind), the magnetospheric dynamics may be significantly different (Cowley, 2013).

The Voyager 2 Planetary Radio Astronomy (PLA) instrument detected bursty radio emissions, referred to as Uranus Kilometric Radiation (UKR), originating from the Uranian nightside, on magnetic field lines which had footprints near the southern magnetic pole (Kaiser et al., 1987). In addition, weak auroral signatures in the form of UV emission from atomic and molecular hydrogen were detected at the Uranian nightside by the Voyager 2 UV spectrometer (Broadfoot et al., 1986). The emission was seen near the Uranian magnetic poles, which due to the large tilt of the Uranian magnetic field nearly coincided with the planetary spin equator. Uranian auroral emissions near equinox have recently been observed from Earth using the Hubble Space Telescope, reporting a different auroral configuration from that seen by Voyager 2 near solstice (Lamy et al., 2012), further highlighting the unique seasonal variability of the Uranian magnetosphere.

The Uranian magnetosphere is host to a robust trapped charged particle population. However, plasma densities are generally low (< 3 cm^{-3}) and ions, with the exception of H^+, were absent above the detection limit of the Voyager 2 Plasma Spectrometer (PLS) (McNutt et al., 1987). The lack of heavy ions has been explained by the fact that due to the highly tilted magnetic field, the population of neutrals sputtered or ejected from the surfaces of the moons is geometrically offset from the plasma population, and thus only very tenuous heavy ion tori are expected (Cheng, 1987). Uranus possesses intense electron and proton radiation belts, and microsignatures due to energetic charged particle interactions with several of the Uranian moons were seen in data from the Voyager 2 Low Energy Charged Particle (LECP) instrument (Mauk et al., 1987).

As previously mentioned, it has also been suggested that subsurface oceans may be present in the moons Titania and Oberon (Hussmann et al., 2006), and due to the highly inclined and thus highly time-variable magnetic field of Uranus, it may be possible to probe these layers by measuring induced magnetic fields (*e. g.*, Saur et al. (2009)).

3. Science Definition

The main open science questions related to the Uranian system have been reviewed in Section 2. Derived from that, Table 2 summarizes the top-level questions and their link to ESA's Cosmic Vision 2015-2025 goals (Bignami et al., 2005).

Table 2: Top level science questions.

Theme	Science question	Cosmic Vision
Atmosphere	What is the composition of Uranus' atmosphere?	1.1, 2.2
	What processes shape Uranus' atmospheric dynamics?	2.2
Interior	What is the internal structure of Uranus?	1.1, 2.2
	Why does Uranus emit so little heat?	1.1, 2.2
Moons and Rings	How did Uranus' moons form and evolve?	1.1, 2.3
	How did Uranus' rings form and evolve?	1.1, 2.3
	How do the moons interact with the magnetosphere?	2.1, 2.3
Magnetosphere	What is the configuration of Uranus' magnetosphere?	2.1, 2.3
	What are the dynamics in the magnetosphere?	2.1

In this section, the precise science questions are listed, the required measurements are defined, and instruments capable of performing these measurements are presented. In Section 3.1 to Section 3.4, the required measurements and potential instruments that could be used to address the top level questions are discussed. In Section 3.5 a payload floor is defined, and, the interrelations between the instruments and their link with top level science questions is identified.

3.1. Atmosphere

The composition of the atmosphere is linked to the bulk composition of the Uranian system, and therefore to the conditions in the Solar nebula. More detailed knowledge of the composition will allow improvements of planetary formation models and could help to better constrain exoplanet studies. The composition of the atmosphere can be measured directly or can be constrained by dynamic modeling. For instance, understanding why Uranus emits such a small amount of heat can only be done in the context of thermodynamic modeling of the atmosphere. Therefore, the atmosphere needs to be characterized from both a composition and a thermodynamic point of view.

The most important chemical information to retrieve is the elemental concentrations, especially of disequilibrium species, isotopic ratios and noble gases, in combination with information regarding the distribution of aerosol particles with depth. These measurements can be made in situ by a probe, which provides high accuracy and depth coverage. The chemical composition of the atmosphere and the isotopic ratios of the major gaseous constituents can be determined in situ from a gas chromatograph coupled to a mass spectrometer. The abundances of water and ammonia in the Uranian atmosphere can be determined with a microwave radiometer, since these elements are strong absorbers at the operational frequencies of this instrument. According to Simões et al. (2012), further information on the abundances of volatiles (water and ammonia) can be obtained by measuring Tremendously Low Frequency (TLF) and Extremely Low Frequency (ELF) waves characteristics, which correspond to a frequency range of 0.3 - 3 Hz and 3 - 30 Hz, respectively. By detecting Schumann resonances in the TLF and ELF wave signatures, the uncertainty of the volatiles abundances can be constrained. The atmospheric concentrations of particles along the probe's descent can be characterized with a nephelometer. The nephelometer can be expected to be sensitive to particles with radii of 0.2 to 20 μm at concentrations of less than 1 cm^3 (Ragent et al., 1992). The aerosol particles can be chemically analyzed by means of an aerosol collector pyrolyzer, to sample and collect the matter, and a gas chromatograph and mass spectrometer, to determine the chemical composition of the sampled particles.

The thermodynamic state of the atmosphere can be characterized by the wind speed distribution, and, density and temperature profiles. The wind speed distribution can be studied by performing high-precision tracking of the probe during its descent, derived from the residual Doppler of the probe's radio link to the orbiter. Additionally, the combination of Doppler and VLBI tracking of the probe signal from ground-based stations can provide a two-dimensional horizontal wind profile of the probe's descent (Witasse et al., 2006). Remote sensing instruments, such as a spectrometer covering the ultraviolet (UV), visible, and/or near-infrared (IR) regions of the spectrum, can provide global coverage and time variations. The density, pressure, and temperature conditions

of the atmosphere can be determined by a combination of sensors, *e.g.*, three-axis accelerometer, Kiel probe, capacitive gauges and temperature sensors, in the probe during its descent in Uranus' atmosphere. Regarding the achievable depth, Falkner et al. (2010) studied the characteristics of a Uranus-dedicated probe, and arrived to a design which would be able to provide measurements down to 100 bars. The thermal state of atmosphere at such depths can be studied by means of a microwave radiometer. Based on the characteristics of the microwave radiometer developed for NASA's Juno mission (Pingree et al., 2008), the vertical temperature profile of Uranus can be measured to an unprecedented depth of up to 200 bars. These results can be achieved with a method known as relative limb darkening (Neckel & Labs, 1994), which surpasses – by far – the expected results of any other known methods. Global coverage can be obtained by remote sensing instruments, such as a thermal or a visible/near-IR spectrometer. When both, global coverage and measurements at depth can be obtained, the best synergy is obtained as one data set provides context for the other.

3.2. Interior

The deep structure of Uranus can be constrained by several categories of measurements. The basic constraints for interior models are the mass distribution, moment of inertia and surface heat flow. Additionally, improvements on the equatorial radius estimate, the flattening factor, the rotation rate and the characterization of the magnetic field can provide strong constraints to internal structure models.

The gravity field of Uranus can be inferred from radiometric tracking data of a fly-by or an orbiter, as the spacecraft's orbit is perturbed by the gravity field of Uranus. The estimation of spherical harmonic coefficients from tracking data is an ill-posed inverse problem. However, repeated tracking at pericenter passage, preferably at low altitudes, and tracking the satellite at various latitudes, will help to better constrain the interior model, which indicates that an orbiter would be better suited for this purpose. In case of having an Uranus orbiter, it will be possible to determine low-degree coefficients with higher precision (J_2 and J_4, Cody & Stevenson (2005)), and eventually to detect non-zero coefficients of higher degree. The gravimetry experiment can be carried out by tracking the spacecraft in X- and Ka- bands with a number of ground stations from ESA's deep space tracking network (ESTRACK) and possibly from NASA's Deep Space Network (DSN). In addition, the Planetary Radio Interferometry and Doppler Experiment (PRIDE) tracking technique, which uses stations from the European VLBI Network (EVN), can be used to further improve the orbit determination (Witasse et al., 2006; Duev et al., 2012). The gravimetry experiment requires onboard X- and Ka band transponders, and an ultra-stable oscillator.

The planet's radius can be constrained by means of occultations of the spacecraft by Uranus and by stellar occultations. The number of radio occultation events needed in order to constrain the radius to a certain accuracy depends strongly on the geometry of the experiment, which can only be assessed once the orbit of the spacecraft is known. The spatial and temporal variation of the magnetic field can be obtained by using a three-axis fluxgate magnetometer onboard the main spacecraft, capable of operating in either vector or scalar mode (Dougherty et al., 2004).

3.3. Moons and Rings

As discussed in Section 2.4, little is known about the Uranian moons and rings. A mission to the Uranian system, especially one with dedicated flybys of the Moons, will greatly increase knowledge in this area. Accurate knowledge of the moons' masses, mass distribution, shapes, tectonics, surface geology and (evolution of) orbital parameters can shed light on their origins and current interactions. These quantities can be measured by a combination of astrometric techniques, using optical imaging systems and spacecraft radio tracking techniques.

The moons can be imaged in the visible region of the spectrum using both narrow angle and wide angle cameras. These cameras can be used to characterize the surfaces of the moons by determining their morphology, and determining the number and size of craters on their surfaces. The resolution should be higher than the highest resolution images obtained with Voyager 2, which were in the order of 2 - 3 km/pixel (Smith et al., 1986). An IR spectrometer can be used to detect sources of heat and to provide constraints to the interior model of these bodies. The composition of the surface can be measured by means of visible and near-IR spectroscopy.

The rings can also be imaged with narrow angle and wide angle cameras. The composition and sizes of particles in the rings, which have been found to vary between meter (in ring ϵ) to submicrometer size (in ring λ) (French et al., 1991; Esposito et al., 1991; Gurnett et al., 1987), can be determined primarily by visible and near-IR spectroscopy. Additionally, the structure of the rings can also be determined with an UV imaging spectrograph, which images the ultraviolet light reflected off the particles of the rings. The dynamics and characteristics, such as mass, velocity, electric charge, and chemical composition, of micrometer-sized particles near the equatorial plane can be determined by means of a dust analyzer, with similar specifications to the Cosmic Dust Analyzer (CDA) developed for NASA/ASI's Cassini orbiter (Srama et al., 2004). Nanometer-sized particles can be characterized

with an electrostatic analyzer, such as the Ion Compistion Analyzer (ICA) developed for ESA's Rosetta mission (Nilsson et al., 2006).

Magnetic field measurements around the moons, with a three-axis fluxgate magnetometer, would have the potential of strongly constraining the interior models of the moons, by detecting the presence or absence of an induced magnetic field, which could indicate the existence of sub-surface oceans or conducting layers.

3.4. Magnetosphere

As mentioned in section 2.5, the magnetosphere of Uranus is atypical, with the magnetic dipole being significantly offset and tilted from the axis of rotation. Its interaction with the solar wind can be determined by probing the magnetic field and charged particles at different times and locations, both crossing the magnetopause and magnetotail. To this end, a polar orbit with high eccentricity is desirable for an ample coverage. In this manner, the configuration and dynamics of the magnetosphere can be characterized, defined as the top-level science questions (see Table 5).

Measurements of the magnetic field can be made with a three-axis fluxgate magnetometer located at the end of a boom. Radio emissions and plasma waves measurements in the magnetosphere can be made with an electric field sensor operating over a range of $\sim$ Hz - MHz, and an assembly of magnetic search coils, providing in this way spectral information for both the electric and magnetic components of the magnetosphere. Additionally, a Langmuir probe can be used for electron density and temperature measurements.

In order to study the Solar wind interaction with Uranus and the internal dynamics of the Uranian magnetosphere, the spacecraft needs to perform in-situ measurements of electrons and ions. By using an ion and electron spectrometer and an ion composition analyser, the three dimensional velocity distribution of these particles can be observed, as well as the mass distribution of ions. For the ion and electron instrument, heritage is taken from the Ion and Electron Sensor (IES) instrument developed for ESA's Rosetta mission (Burch et al., 2006), which is capable of detecting positively and negatively charged particles from 1 eV/e to 22 keV/e with an energy resolution of 4%. For the ion composition analyser, heritage from Rosetta's ICA sensor is taken, which is capable of detecting ions with energies of 25 eV/e to 40 keV/e with an energy resolution of 7% (Nilsson et al., 2006). Rosetta's ICA is capable of resolving H^+, He^+, He^{++},O^+, O^{++} and CO_2^+ ions, and is also sensitive to N^+, H_2O^+ and O_2^+ and would thus be a suitable candidate for measurements of ions of Uranian and Solar Wind origin.

Further science with regard to the magnetosphere can be carried out by measuring energetic particles with an energetic particle detector. This instrument should be capable of detecting electrons from 15 keV to 1 MeV and H to Fe ions from 15 keV/nucleon to $\sim$ 3 MeV/nucleon, based on the Energetic Particle Spectrometer (EPS) instruments onboard the MESSENGER and New Horizons spacecraft (Livi et al., 2003; McNutt et al., 2009). Finally, the optical remote sensing techniques, visible and near-IR imaging, and UV spectroscopy, can be used to study the interaction of the Solar wind with the Uranian magnetosphere by observing auroral emissions.

3.5. Payload floor

From the set of instruments mentioned in Section 3.1 to 3.4 a baseline payload floor is defined, which has been summarized in Table 3, for the main spacecraft, and Table 4, for a potential probe. Additionally, Tables 3 and 4 provide details regarding the heritage, and the measurement range and sensitivity of the instruments used as a reference. It should be noted that the exact number of samples, resolutions, images, and cadences of the instruments have not been determined as part of this study. The traceability matrix, presented in Table 5, shows the interrelations between the instruments, the importance of each instrument in performing a given measurement, and the importance of a measurement for answering each of the top level science questions. These values will be used in Section 4 for the mission concept definition and trade-off. As shown in Table 5 with the current baseline payload, all the top level science questions are addressed. The different science-based descoping scenarios to the baseline payload and their effect in the science return, have not been analyzed as part of this study.

Table 3: Potential instruments for spacecraft.

Instrument	Heritage	Description	Range
VINIRS	Dawn *VIR*	Visible and Near Infrared Spectrometer	λ : 0.25 - 5 μm 96 bands (1.8 nm per band)
IRS	Cassini *CIRS*	Thermal Infrared Spectrometer	λ : 7.16 - 16.67 μm 1×10 array of 0.273 mrad squares
UVIS	Cassini *UVIS*	Ultraviolet Imaging Spectrograph	λ : 55.8 - 190 nm
RPW	Cassini *RPWS*	Radio and Plasma Wave Instrument	1 Hz - 16 MHz (various channels)
MAG	Juno *MAG* Swarm *VFM*	Fluxgate Magnetometer	Dual 3 axis <1 nT accuracy range of 0 - 20000 nT
TELFA	C/NOFS *VEFI* antennas	TLF and ELF Antenna	Schumann resonances TLF and ELF frequencies
ICI	Rosetta *ICA*	Ion Composition Instrument	Positive ions from 25 eV to 40 keV (dE/E = 0.07)
EIS	Rosetta *IES*	Electron and Ion Sensor	Electrons and ions from 1 eV/e to 22 keV/e (dE/E = 0.04)
EPD	New Horizons *PEPSSI*	Energetic Particle detector	Protons: 15 keV - 3 MeV Alphas: 25 keV - 3 MeV CNO: 60 keV - 30 MeV Electrons: 15 keV - 1 MeV
NAC	Cassini *ISS*	Narrow Angle Camera	Res: 6 μrad/pixel Spectral range: 350 - 1050 nm
WAC	Cassini *ISS*	Wide Angle Camera	Res: 60 μrad/pixel Spectral range: 350 - 1050 nm
RSE	Cassini *RSS*	Radio Science Experiment	USO Allan deviation at $\tau = 100$ s of 1×10^{-13} Transponders operating at S, X and Ka band.
MWR	Juno *MWR*	Microwave Radiometer	0.6 - 22 GHz Gain up to 80 dB Temp. Profile up to 200 bars
DC	Cassini *CDA* New Horizons *SDC*	Dust Analyzer	Particle mass range: 10^{-15} - 10^{-9} kg, Particle size range (radius): 1 - 10 μm.

Table 4: Potential instruments for probe.

Instrument	Heritage	Description	Range
DWE	Huygens *DWE*	Doppler Wind Experiment	dv = 1 m/s Depth: 20 bars
AP3	Huygens *HASI*	Atmospheric Physical Properties Package	Temperature, pressure and density profiles Depth: 0 - 20 bars
GCMS	Huygens *GCMS*	Gas Chromatograph and Mass Spectrometer	Heavy elements, noble gases, key isotopic ratios (H_2/He, D/H, PH3, CO) and Disequilibrium Species
AS&NEP	Galileo *GPNE* Huygens *ACP*	Nephelometer and Aerosol Sampling System	Particle size range (radius): 0.2 to 20 μm, at concentrations of $< 1\,cm^3$

Table 5: Traceability matrix, showing selected instruments, with the relative importance of each measurement for answering the different science questions.

Top level science theme	Question	Measurement		SPACECRAFT INSTRUMENTATION													PROBE INSTRUMENTATION			
			Question priority (3=High)	VINIRS	IRS	UVIS	RPW	MAG	TELFA	ICI	EIS	EPD	NAC	WAC	RSE	MWR	DC	DWE	AP3	GCMS	AS&NEP
Atmosphere	What is the	Noble gases	3																	3	
	composition	Isotopic ratios	3																	3	
	of Uranus'	Elemental abundances	3	2	2											2				3	
	atmosphere?	Disequilibrium species	2	1	2															3	
	Why does Uranus emit so little heat?	Thermodynamic profile	3		1										1	3			3		
	What processes	Atmospheric motions	2	3	3	2							3	3		3		3			
	shape Uranus'	Atmospheric conductivity	1						2										3		
	atmospheric dynamics?	Cloud distribution	1	3	3										1	1					3
Interior	What is	Gravity field	3												3						
	the internal	Radius at 1 bar	3												3						
	structure	Magnetic field	1					3													
	of Uranus?	Electromagnetic attenuation	1						3												
		Rotation rate	3	1			3	3					1								
Magnetosphere	What is	Particle populations	3				1			3	3	3									
	the configuration	Magnetic field	3				3	3													
	of Uranus'	Radio emissions	2				3														
	magnetosphere?	Plasma waves	1				3														
	What are the dynamics	Energy transport	2				2	3		3	3	3									
	in the magnetosphere?	Solar wind interaction	2	1		1	2	3		3	3	2	2	1							
Moons & Rings		Surface composition	3	3		1															
	How did	Size and shapes of moons	3										3	2							
	Uranus'	Cratering history	3										3	3							
	moons form	Surface morphology	2	1	1								3	2							
	and evolve?	Surface: physical properties	1	2	3								1	1							
		Magnetic fields	2					3													
		Gravity field, internal structure	3												3						
	How did Uranus' rings	Composition of rings	2	3													2				
	form and evolve?	Size of ring particles	1	2		3							1	1			3				
		Rings dynamic	1	2									3	2							
	How do the moons interact	Exospheres	1					3	3	3	3	2					1				
	with the magnetosphere?	Solar wind interaction	1	3	2	1	3	3		3	3	3									

Key
3 - Essential instrument
2 - Important instrument
1 - Useful instrument

4. Mission Architecture Trades

In this section, the generation of possible mission concepts and the selection process of the optimal architecture are presented. First, the formulation of the concepts will be presented in Section 4.1, including an initial reduction of possible mission concepts. Subsequently, the trade-off process and rationale for the science and engineering performance of the remaining concepts will be discussed in Section 4.2. Finally, the results of the trade-off will be presented in Section 4.3.

4.1. Concept generation

The design process started by generating top-level mission architecture options. From the various combinations of these options, an initial set of mission architectures is created. From this initial set of architectures, several steps are taken to reduce the number of concepts that are considered, resulting in a set of concepts that are deemed most feasible and competitive. These concepts are subsequently compared in a more detailed manner in Section 4.2, considering the specific engineering constraints, instrument packages, and resultant science return.

Generating the mission concepts was achieved by defining several top-level characteristics and combining them where possible. This yields a possible mission concept for each feasible combination. The following aspects were considered:

- **Flyby or orbiter mission**: A flyby mission would have the advantage of lower complexity and time-of-flight, and therefore cost, at the expense of science return. On the other hand, an orbiter would allow for much greater spatial and temporal resolution of the data gathered with the instruments, as much greater and longer coverage of targets of interests is available.
- **Simple spacecraft, intermediate spacecraft or high-performance spacecraft (roughly 50 kg, 100 kg and >100 kg payload mass, respectively)**: The size class of the total spacecraft mass is driven strongly by the corresponding payload mass. This differentiation corresponds effectively to science return, assuming a given mission architecture. However, a higher payload mass for a given mission architecture will result in a higher total system mass and higher cost.
- **Zero, one, or two atmospheric probes**: An atmospheric probe would provide valuable in-situ measurements (see Section 3.1) of the Uranian atmosphere. Multiple probes would provide spatial resolution for the in-situ measurements, as well as mitigate the risk associated with the possibility of entry at abnormal atmospheric conditions.
- **Single or multiple orbiters mission**: Multiple orbiters would provide superior data for magnetosphere dynamics by making concurrent measurements at separated points in the magnetosphere.
- **Inclusion of a satellite tour**: A tour of Uranus' satellites would increase the knowledge of these bodies (see Section 3.3) since measurements could be taken from much closer distances. However, there is little possibility for using satellite gravity assists to the degree that Cassini does at Saturn, because the Uranian moons are considerably smaller than Titan. As a result, including a moon tour would require a substantial ΔV investment.

The resulting number of feasible combinations that is obtained from this list has been decreased to a number at which a quantitative trade-off can be performed, from both an engineering and a scientific point-of-view, with a reasonable amount of effort. This initial selection was made by considering the most competitive mission from various perspectives, based on engineering feasibility and science value.

For making this selection, a number of assumptions on available systems have been made. For instance, the availability of the Ariane 5 Midlife Evolution (ME) launcher has been assumed for some scenarios, allowing the feasibility of heavier and shorter travel-time mission concepts. Additionally, the possibility of having a steerable antenna or scanning platform, which would enable the system to perform both radio science and remote observations simultaneously during the close flybys, was discarded as a design option. This choice was made due to the substantial risk and uncertainty involved in the use of such a system. It is not deemed to be a competitive solution at this point in the design process, since the failure of the scanning platform would present an additional failure mode with high consequences and relatively large probability of occurrence, due to the limited experience with such systems (especially on long-duration missions). The lack of scanning platform could strongly influence the feasibility of certain concepts, however. Especially for the flyby, where only a single chance for measuring is available, this has severe implications. For the orbiter concepts, both Uranus and its moons (if applicable) can be flown-by many times (see Section 5.5), so that the added value from additional

Table 6: Summary of selected mission concepts.

Concept #	Encounter type	Spacecraft size class	Number of probes	Number of spacecraft	Satellite Tour
1	Flyby	High performance	1	1	No
2	Orbiter	Small	2	1	No
3	Orbiter	Intermediate	1	1	Yes
4	Orbiter	Intermediate	1	1	No
5	Orbiter	Intermediate	0	2	Yes
6	Orbiter	Intermediate	1	2	No

sets of observations of all instruments would be incremental rather than doubling it. However, the possibility of a scanning platform could be investigated further in a subsequent study phase of this project, analyzing the strongly interrelated engineering, science, and planning issues.

The key science and engineering criteria for selecting the most competitive design options are summarized in the following. In addition, it was considered important to have a diverse set of mission concepts to explore further, so that the design space is comprehensively explored in this initial phase:

- For a flyby mission, only a high-performance orbiter (*i.e.*, with a large payload suite) was considered further, since only such a spacecraft was deemed to have sufficient capability for flyby-only science return to warrant its development. Similarly, a probe was deemed crucial for a flyby mission, as the science return from a probe is similar for an orbiter or flyby mission.
- The high performance (*i.e.* the spacecraft with payload mass $>$ 100 kg) orbiter was deemed unfeasible for orbiter missions due to excessive mass and therefore cost requirements.
- For the multi-spacecraft concepts only an intermediate orbiter with a magnetospheric-science-dedicated payload package on the secondary craft was considered, because other payload packages for multiple spacecraft do not warrant the added complexity. For this combination, both a satellite tour and a probe addition, is considered.
- For the simple orbiter, only the two-probe option was considered, as it was deemed the most competitive one for the class of mission that is considered here. An example of a simple orbiter-only mission is Uranus Pathfinder (Arridge et al., 2011), albeit without entry probe(s).

The final six concepts are summarized in Table 6.

4.2. Trade-off process

Having defined the most competitive design options, given in Table 6, the science return and engineering issues of each concept are now investigated. The results were used to perform trade-offs for both the science and engineering aspects described in Sections 4.2.1 and 4.2.2, respectively. These trade-offs have been performed separately, resulting in two scores (science and engineering) for each concept. The methodology used for combining these scores and selecting the final concept is described in Section 4.3.

4.2.1. Science trade-off

The science return of an interplanetary mission is typically the major driver in its selection. As such, a thorough analysis of the science that can be done with a given mission concept is crucial. Section 3 defined the set of instruments that were determined to be best suited for answering the science questions, depicted explicitly in the traceability matrix (Table 5) .

For the science trade-off, this matrix was used to generate scores for each instrument representing their ability to answer each of the science questions. These were then weighted to include the importance of each of the questions in each of the science themes. These results, combined with considerations of the instrument mass, were used to select payload packages for each of the six different possible mission architectures. The result of this selection is shown in Table 7.

Having selected the payload for each mission concept, the final trade-off is performed by comparing the performance of the instruments in the different mission architectures. This comparison is combined with the

Table 7: Selected model payload per mission concept.

Instrument	Mass [kg]	Heritage	(1)	(2)	(3)	(4)	(5)	(6)
Total mass budget [kg]:			150.0	50.0	120.0	120.0	120.0	120.0
Total mass budget less 20% margin [kg]:			125.0	41.7	100.0	100.0	100.0	100.0
VINIRS	11.0	Dawn	11.0		11.0	11.0	11.0	11.0
IRS	30.0	Cassini	30.0		30.0	30.0	30.0	30.0
UVIS	4.4	New Horizons	4.4					
RPW	9.0	Cassini	9.0	9.0	9.0	9.0	9.0	9.0
MAG	11.0	Juno	11.0	11.0	11.0	11.0	11.0	11.0
ELFA	2.0	C/NOFS	2.0	2.0	2.0	2.0	2.0	2.0
ICI*	5.7	Rosetta	5.7	5.7	5.7	5.7	5.7	5.7
EIS*	3.6	Rosetta	3.6	3.6	3.6	3.6	3.6	3.6
EPD	3.0	New Horizons	3.0	3.0	3.0	3.0	3.0	3.0
NAC	8.6	LRO	8.6	8.6	8.6	8.6	8.6	8.6
WAC	4.5	Rosetta	4.5					
RSE		Cassini						
MWR	14.0	Juno	14.0		14.0	14.0	14.0	14.0
DC	1.6	New Horizons	1.6					
Total payload mass [kg]			108.4	42.9	97.9	97.9	97.9	97.9

*Mass includes part of Data Processing Unit shared by ICI and EIS

importance of the measurements of a given instrument to answer a given science question, and its associated weight, shown in Table 5.

What remains is to determine the difference in how well an instrument can be used for answering a given science question in each of the mission architectures. To include the architecture-dependent performance of the instruments in the trade-off, a relative score per instrument level is generated, comparing the performance of each instrument for each science question it contributes to, for each mission architecture.

The bulk of the difference in determining the relative performance of each instrument can be derived from the following considerations.

- The small orbiter with two probes would answer the questions in atmospheric science with the highest accuracy and with higher certainty. However, due to a smaller overall payload, it scores relatively low in most other categories.
- The same set of instruments could be used more effectively to answer moon origin and formation questions in the architecture options which include a tour of the moons.
- The same set of instruments could be used more effectively to answer magnetosphere questions in the architecture options which include a slave satellite.
- A given instrument on the flyby mission generally has a lower capability to be used to answer a given science question, since the spatial and temporal variability of achievable data would be less than for an orbiter mission. However, the science return from probe instruments are not reduced by the same extent. A reduction in efficiency of probe instruments is assumed, since there is less possibility for remote sensing instruments to put the probe measurements into perspective for the case of the flyby mission.
- The highly limited bandwidth for transmitting data back to Earth was considered, since the amount of data that can be collected with any of the instrument suites cannot all be transferred to Earth, and some selection and sampling methods will be needed. However, this consideration has no impact on the flyby mission. Although the total amount of data that will be collected by a flyby mission will be lower than for an orbiter mission, due to the limited time that can be spent collecting data, it will not suffer similar data rate bottleneck. Instead, the total data is limited by the short flyby duration.

The differences between the concepts, from a science return point-of-view, is now reduced to two steps. First, the instrument suite is different for each concept. Second, the degree to which a given instrument can be used to answer a given science question is different between the concepts. Using the traceability matrix, these considerations are weighted and combined to obtain a science score for each concepts.

By using this process, several levels of choices and trade-offs were combined, weighting the science themes, the importance of a science question in a science theme, the selection of instruments for a given concept and the ability of each instrument to answer a given question in a given mission concept. This process contains a combination of qualitative and quantitative considerations, which is inherent in conceptual design. As a result,

the trade-off scores should not be seen as absolute and missions with similar scores cannot be unambiguously distinguished in terms of optimality. However, it should be noted that the qualitative considerations should be quantified as much as possible in further design phases and subsequent design iterations should be updated accordingly.

Our process has resulted in a science trade-off score for each mission concept, normalized with the orbiter with probe and moon tour concept (benchmark) score, resulting in the following scores:

- Concept 1 (flyby with probe): 66%.
- Concept 2 (small orbiter, and two probes): 79%.
- Concept 3 (orbiter with probe, and moon tour): 100%.
- Concept 4 (orbiter with probe): 88%.
- Concept 5 (orbiter, slave satellite, and moon tour): 88%.
- Concept 6 (orbiter, slave satellite, and probe): 99%.

The flyby architecture was found to have the lowest score, motivated strongly by its very low temporal and spatial variability of measurements, as well as the higher focus on specific measurements, due to the smaller observation time. The small orbiter also scored relatively low, as was to be expected due to its reduced instrument suite. The mission concepts that incorporate a slave satellite scores relatively low, due to the lower priority score given to the magnetosphere theme. The benchmark concept scores highest, as it is the most well rounded in terms of science return, being mostly in terms of magnetospheric science (due to the absence of a slave satellite). However, due to the low relative weight of magnetospheric science in this mission design, this does not unduly influence the science score.

4.2.2. Engineering trade-off

Although the mission design is driven by its potential science return, it must be performed within constraints imposed by the current level of technology, available budget, and the degree of risk that is deemed acceptable. Additionally, factors inherent to the individual mission designs that are not necessarily related to the science return must be included in the trade-off. This could be, for instance, programmatic issues, or the resulting advancement of technology, which are of interest to a space agency carrying out the mission.

For this study, the analyses were performed largely in a top-down manner, where general characteristics of the mission were compared. Where possible, this was backed up by conceptual design calculations. Where more detailed evaluations were not possible, either by nature of the evaluation criteria or the uncertainty involved in the definition of trade-options at this early stage, comparisons to existing mission and heuristic arguments were used in the concept analysis. Matters that could be compared in a quantitative (although conceptual) manner include the time-of-flight, required ΔV, mass estimates, cost and launcher selection.

A weighted Pugh (decision) matrix was selected for evaluating the trade space. By using this method, the six design options are each given a relative score on a number of criteria. Relative weights of these criteria are then used to combine the scores to a final weighted design score.

All criteria are evaluated on a relative scale from one to five with half grades (shown in Table 8), with the exception of the cost score, which is obtained directly from the quantitative method defined by Peterson et al. (2008) and is rounded to the nearest decimal.

The following five criteria are considered in the comparison:

- Cost: The total life cycle cost of the mission is considered a crucial trade criterion because it is decisive for whether a mission would fly or not. For the cost estimation, the method presented by Peterson et al. (2008) is applied for each of the six concepts. The results provide a range of costs between \$1.0B and \$1.3B which are translated to trade-off scores between 1.5 and 3.5. The full range of scores (1 to 5) was not used to reflect the relatively small range of cost values of the five missions. The maximum score of 3.5 (as opposed to 5) was used to reflect the fact that all missions carry a high cost and no 'cheap' option exists.

- Complexity: This criterion encompasses issues that define how difficult and risky the mission will be to design, build, and operate. This comprises matters such as constellation and communications problems when bringing multiple probes, but also more general matters such as the risk of (partial) mission failure due to a high degree of experimental technologies.

- Programmatics: In scope of this study, programmatics are to be comprised of matters related to the design and operations processes, such as the risk for schedule delays or the possibility that the selected launcher is unavailable. Additionally, concepts with an inherently longer and more arduous development process score lower on this scale. Note that this criterion does not directly include any cost overrun risks, as this is covered by the first criterion.
- Technological advance: One of the major roles of space agencies, in addition to the scientific exploration of space, is to advance technology. A mission that pushes further in this respect is more valuable to the space industry. This is why the technological advancement potential is used as a trade criterion, though at low relative weight.
- Public outreach: Planetary missions will deliver fascinating scientific results and inspiring imagery, and their results will also inspire the public, potentially fostering the economy and science, by motivating youth to engage in STEM professions. This is taken into account for the trade at a low weight.

The engineering trade-off is tabulated in Table 8, where the weights of each of the criteria defined above are specified. Cost was deemed the most crucial engineering driver, followed by mission and design complexity, as these two criteria encompass the majority of major difficulties in the design and development of a space mission. Note that the assumed launcher per mission scenario is explicitly mentioned, because it influences many of the criteria. As an example, an Ariane 5 ME is considered to add significant programmatic risk, because its development is still ongoing and there is an inherent risk in assuming its availability

Table 8: Pugh-matrix for the engineering trade-off. ECA stands for Ariane 5 ECA, ME for Ariane 5 ME.

		Architecture/ID					
Criterion	Weight	(1)	(2)	(3)	(4)	(5)	(6)
Cost	1	3.5	3.2	1.7	1.8	2.0	1.5
Complexity	0.75	5	3	3	4	2.5	2
Programmatics	0.5	4	3	4	5	4	2
Technological advance	0.25	4	3	4	4	4	5
Public outreach	0.1	2	2	3	2	4	5
Assumed launcher		ECA	ME	ME	ECA	ECA	ME
Sum		10.45	7.9	7.25	8.5	7.257	5.75
Normalized to (3)		144%	109%	100%	117%	100%	79%

The results are normalized to concept (3), which was selected as the benchmark mission scenario, and was also proposed in the NRC Decadal Survey (Squyres et al., 2011). The very short flyby mission scores best, due to its relatively cheap and simple design and operations, whereas the very complex mission with a sub-satellite and an entry probe scores worst. Options (3) and (5) have very similar scores, underlining that bringing a probe or a slave satellite present similarly difficult, although very different, engineering challenges. The cost of developing a probe will be substantially higher than that of a slave satellite, due to the very limited existence of recent experience and facilities for designing and developing planetary probes, as well as the large uncertainties in the characteristics of Uranus' upper atmosphere. However, probe operations only impose in-system operational and cost requirements at the insertion phase, making the primary mission less complicated to operate and develop than that of a mission incorporating a slave satellite. Upcoming experience with the BepiColombo mission, which utilizes a slave satellite, may allow a better understanding of the complexities involved in multi-spacecraft planetary missions, though. However, as it will be discussed in Section 4.3, the missions with slave satellites do not have a very strong combined score, due to the low emphasis on magnetospheric science. As such, for the study at hand, minor variations of relative engineering scores of a probe or slave mission do not influence the final mission selection.

4.3. Trade-off results

The results presented in Sections 4.2.1 and 4.2.2 provide a separate trade-off score from a science and engineering point-of-view, respectively. In this section, the full trade-off is presented by combining these two categories. When selecting a mission design from these two science scores, the outcome will typically be different when considering different types of missions. For instance, a technology demonstrator mission will place a higher value on

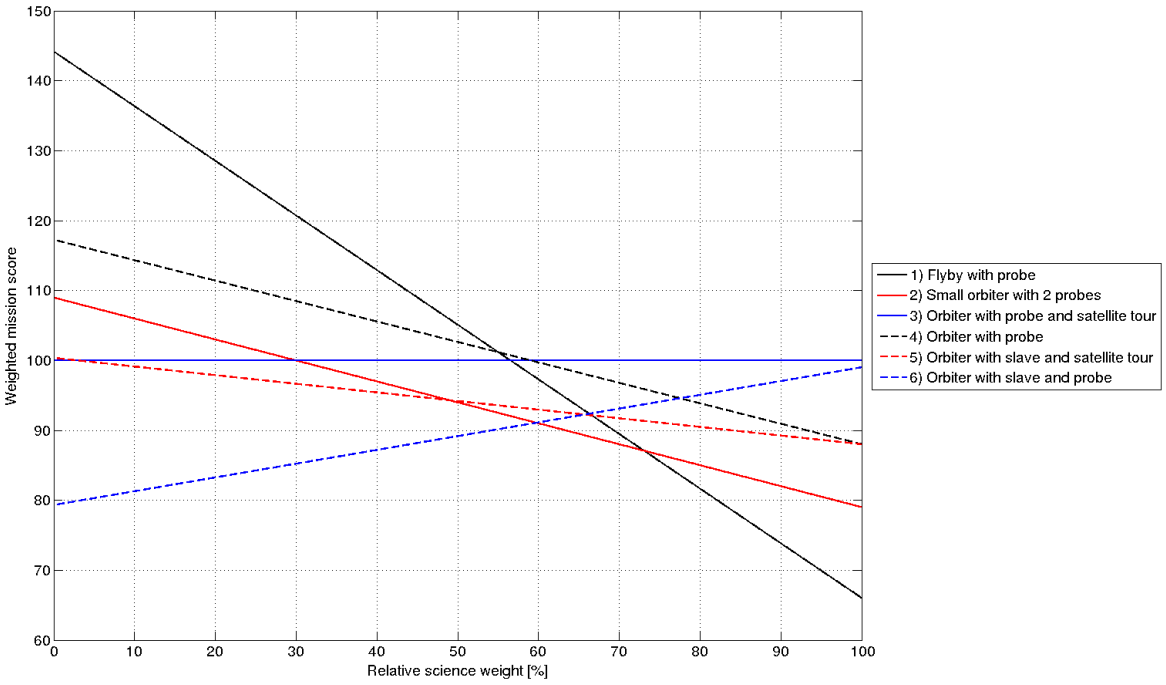

Figure 1: Final scores of mission concepts as a function of relative science and engineering weight.

engineering performance, whereas a flagship science mission will place a higher emphasis on science performance. Here, the full range of relative science and engineering importance in the trade-off process is investigated.

To this end, relative weights are defined for the science and engineering criteria, η_s and η_e, respectively, with:

$$\eta_s + \eta_e = 1 \tag{1}$$

The total mission score C_{tot} for a given concept is then obtained from the science and engineering score, denoted C_s and C_e, respectively, from the following:

$$C_{tot}(\eta_s) = C_s\eta_s + C_e(1-\eta_s)\,(= C_e + (C_s - C_e)\eta_s) \tag{2}$$

As a result, the engineering score C_e generated in Section 4.2.2 is given for Relative science weight η_s= 0% and the science score generated in Section 4.2.1 is given for Relative science weight η_s = 100%. The intermediate relative science weights are obtained from the linear interpolation in Eq. 2.

The results for the combined trade-off are shown graphically in Figure 1. In this figure, trade-off results are shown for the six concepts described in Section 4.1 as a function of η_s, normalized with the orbiter with probe and satellite tour concept. In this manner, the range of science weights where certain mission concepts can be considered to be competitive are identified.

The graph shows a clear change in optimal concepts as a function of the relative weights. Taking into account the fact that the trade-off results should be considered to include a certain degree of uncertainty, most notably due to qualitative considerations used in generating the trade-off scores, concepts with very similar results cannot be distinguished. However, it should be realized that all of the missions will have a substantial science return, as well as require a substantial engineering effort. As a result, the differences between the missions, as observed in Figure 1, are limited to a certain range. Optimal concepts can be identified per "regime" of weight factors:

- For high engineering weights, the results clearly show the desirability of a flyby mission and, to a lesser degree, the orbiter with probe mission. This conclusion holds up to a relative weight of 0.5, indicating the flyby as a competitive mission concept for a program with a stronger emphasis on fast and cost-effective mission development. Alternatively, it would be competitive for a precursor or technology demonstration mission (although most likely in a reduced cost class).

- For higher science weights, from a science weight of 0.6 to 0.7, the flyby mission loses its competitive edge. The orbiter with probe, either with or without a satellite tour, is the most competitive mission concept in this range, with only a marginal difference between the two. Interestingly, the other four mission concepts have a roughly equal score. This indicates two "tiers" of optimal missions at this level. The implication of this is that the four lower scoring missions can be justifiable, but only for a more specialized science focus in which one of these concepts is especially strong. It must be stressed that this regime of weight factors (~ 0.7) is typical for a general mission concept, since for a typical mission the science drives the overall design and is constrained by engineering requirements.

- For very high science weight (near 100%), the orbiter with both a slave and a probe becomes a strongly competitive mission concept, similar in score to the orbiter with probe and satellite tour.

It must be noted that the relatively low outcome of both mission concepts with a slave satellite, which is highly advantageous for magnetosphere dynamics measurements, is driven by the low weight given to magnetospheric science in the weighting scheme, as described in Section 3. For a dedicated magnetospheric mission concept, this weight would increase. For instance, increasing the magnetospheric weight to 3 (equal to atmosphere and interior), makes the orbiter with slave and probe competitive from an engineering weight of 30% downwards. Additionally, it results in a marginal difference between the orbiter with probes and satellite and tours, and the orbiter with slave and satellite tour.

The choice of not having a scanning platform for concurrent radio science and Uranus observation (see Section 4.1) has decreased the science return of the flyby mission. However, the inclusion of such a system would considerably reduce the engineering attractiveness of such a concept. Specifically, the risk associated with such a system, especially for a flyby mission where there is only one chance for making observations, was deemed unacceptable.

Taking a typical relative science weight of 70%, representing a mission driven by science, but taking into account the technological and economical limitations, the orbiter with probe and satellite tour is selected. Although very similar in outcome to the concept without a moon tour, the selected mission profile was deemed the most well-rounded option. If the mission development would indicate that it is not feasible, for instance due to cost constraints, a down-scaled option could be considered, eliminating the moon tour.

Qualitatively, the selected concept provides a balanced science return, focusing on the interior and atmospheric science questions, but taking advantage of the presence in the Uranian system to perform detailed observations of its satellites. The magnetospheric science questions will not be addressed in as much detail, because the analysis showed that an orbiter scenario with both, a probe and a sub-satellite, is an undesirable architecture.

In summary, the mission will consist of a Uranus orbiter with a payload mass of 100 kg (see Table 7), in addition to a 300 kg atmospheric entry probe. The mission will be launched on an Ariane 5 ME launcher and uses a high-thrust chemical propulsion system for Uranus orbit insertion, course corrections, and orbit modifications. In the Uranus system, the satellite will perform close flybys of Uranus' five major moons. The orbit analysis and planning will be further discussed in Section 5. System and subsystem design will be addressed in Section 6.

5. Mission Analysis

In this section, the orbit design process is described. First, the mission requirements and constraints will be presented in Section 5.1. Subsequently, the computation and selection of the Earth-Uranus transfer orbit will be treated in Section 5.2, the analysis of launch opportunities and launcher selection in Section 5.3, the release strategy and orbital characteristics of the probe in Section 5.4, and the design of the Uranus science orbit and moon tour in Section 5.5. In Table 14, the calculated ΔV budget for the entire mission is given, based on the design rationale discussed in Sections 5.2 to 5.5. In Sections 5.6 to 5.7 the logistics concerning the ground segment, orbit determination, End Of Life (EOL) and planetary protection will be discussed.

5.1. Mission requirements and constraints for orbit design

The orbit design process is driven by a set of requirements and constraints derived from the mission concept, which were taken as guidelines for the orbit design. These are:

- The propulsion system for the Earth-Uranus transfer shall be chemical.
- The gravity assists performed shall comply with the required clearances (*i. e.*, distance from central bodies, radiation tolerance), to ensure the safety of the spacecraft while performing these maneuvers.
- The system shall be able to deliver a spacecraft, composed of an orbiter and a probe to Uranus' orbit, having the shortest interplanetary transfer possible (refer to Section 4.3 for the rationale of this requirement).
- The probe shall be released before insertion into a Uranus-dedicated orbit.
- The Uranus-dedicated orbit shall be suitable for carrying out all the proposed scientific measurements. For instance, it shall allow the orbiter to perform both, gravimetry and magnetospheric measurements (*e. g.*, low periapsis and high apoapsis altitudes).
- Aerocapture shall not be considered for orbit insertion, due to the low Technology Readiness Level (TRL) of this technique.
- After the Uranus science dedicated orbit, a moon tour around Uranus' five largest moons shall be conducted (refer to Section 4.3 for the rationale for this requirement).

5.2. Interplanetary Transfer Orbit

The transfer orbit scenarios were firstly assessed based on the study of Strange & Longuski (2002), in which different viable gravity-assist sequences for multiple targets were identified using an analytical technique derived from Tisserand's criterion. Each option was analyzed by performing a trajectory optimization using the differential evolution algorithm implemented in the software tool PaGMO (Parallel Global Multi-objective Optimizer)(Biscani et al., 2010).

From this analysis, it was concluded that the best option is to insert the spacecraft into an interplanetary transfer orbit with a Venus-Earth-Earth-Jupiter (VEEJ) sequence of gravity assists with the characteristics stated in Table 9. Other studies like Arridge et al. (2011) and Squyres et al. (2011) demonstrate that shorter transfers are available in 2021 (13 to 15 years). However, the current mission concept does not consider those dates as realistic for launch. Additionally, the dry-mass ratio available for such transfers would not be enough to comply with the main mission requirement, which is to deliver an orbiter and a probe to the Uranus system.

Table 9: The selected VEEJ sequence.

Sequence	C3 [km^2/s^2]	Transfer Duration [yr]	V_{esc} [km/s]	ΔV_{DSM} [km/s]	V_∞ [km/s]	Total ΔV [km/s]	Dry Mass [kg]
VEEJ	12.04	17.40	3.47	0.10	6.20	2.05	2553.52

5.3. Launch

The mission baseline launch is set to be on September 14, 2026, which corresponds to the option with the lowest C3 and total ΔV, in the feasible time frame. The lower and upper limits of the launch window were obtained based on two considerations: the launch vehicle shall deliver a minimum dry mass of 2000 kg to Uranus orbit and the time of flight shall be under 20 years. The first consideration set the upper limit of the launch to October 1, 2026, and the second consideration set the lower limit to September 10, 2026, resulting in a 21-day launch window. In case of an extensive delay of the mission, an alternative launch date would be in November 2029, 38 months after the baseline. A similar launch window could be established for this date.

In addition to the launch window and the delayed launch option, launch profiles have been analyzed for a descoped and an enhanced mission in terms of deliverable dry mass to the Uranus system. The launch opportunities analysis is summarized in Table 10.

Table 10: Launch energy, time of flight and launcher performance values for the 21-day launch window and backup launch scenario.

Concept	Launch Date	C3 [km^2/s^2]	Total ΔV [km/s]	Arrival Date	Transfer Duration [yr]	Dry Mass* [kg]
Launch window start	10-Sep-2026	12.25	2.06	10-Feb-2044	17.42	2529.19
Nominal launch window	14-Sep-2026	12.04	2.05	11-Feb-2044	17.41	2553.52
Launch window end	01-Oct-2026	15.00	2.06	24-Feb-2044	17.40	2420.96
Enhanced mission	09-Sep-2026	11.70	1.56	29-Apr-2046	19.72	3019.70
Descoped mission	05-Aug-2026	9.18	3.08	16-Jan-2043	16.45	2109.68
Delayed mission	02-Nov-2029	10.43	2.11	31-Aug-2049	19.83	2692.84

*Including margins.

5.4. Probe

Twenty days before entry, the atmospheric probe separates from the spacecraft. This separtion time was adopted based on the Uranus-dedicated probe study presented in Falkner et al. (2010). The spacecraft performs an orbiter deflection maneuver of 20 m/s to target the entry point on Uranus. The probe is spun at an attitude required for entering the atmosphere. For the study at hand, the V_∞ at Uranus is 6.2 km/s, and the entry velocity at the interface altitude of 700 km is $\sim$ 21.8 km/s.

The flight path angle for the selected entry point will be $\sim$ 35 deg, which is tolerable for the probe from an aerothermodynamics point of view (Falkner et al., 2010). The entry and descent are visible from both, the Earth and the spacecraft. The flight path of the probe also avoids the potentially hazardous region of the Uranian rings situated within a radius of 2 R_U on the equatorial plane of Uranus.

The distance between the probe and the spacecraft is approximately 55000 km at the start of the probe's entry and descent. This distance is within the range of the UHF antennas of the probe (see Section 6.3). The probe collects data from a range of 0.1 to 100 bars of pressure for 90 minutes. The probe descent phase is completed half a day before orbit insertion of the orbiter, providing enough time for preparations for the orbit insertion maneuver.

5.5. Uranus Science Orbit and Moon Tour

The Uranus orbit insertion is carried out by performing a ΔV burn of 1.01 km/s at the point of closest approach to the planet, at a distance of $\sim$ 1.2 R_U, avoiding the hazardous ring area. After orbit insertion, the Uranus science phase commences.

5.5.1. Uranus Science Orbit (USO)

In order to design the Uranus Science Orbit (USO) the following considerations were taken into account:

- A highly elliptical orbit is desirable in order to reduce the ΔV for orbit insertion.
- The orbiter should be able to reach a wide range of altitudes with respect to Uranus' surface, in order to comply with the different science objectives (*i. e.*, low altitudes for gravimetry and atmospheric studies, and high altitudes to be able to cross Uranus' magnetopause for magnetospheric investigations).
- The periapsis passage should be visible from Earth.

- The orbit should be polar (or close to polar) to provide a better Uranus coverage for gravimetry and atmospheric studies.
- The hazardous rings of Uranus, situated within $2\,R_U$ on the equatorial plane of Uranus, should be avoided at all times.
- The orbit should be designed so that there is enough time allocated for data transmission back to Earth, with the expected low data rates (see Section 6.2).

Having taken into account these requirements and constraints, the Uranus science orbit was chosen to be a highly elliptical polar orbit, with a periapsis of $1.2\,R_U$ and an apoapsis of $60\,R_U$. The period of this orbit is 20.2 days. The orbiter will remain in this orbit for approximately two years, in which the spacecraft will complete 36 orbits around Uranus. In Section 3 the science objectives of this phase are summarized. This phase will be referred to as the USO phase throughout the rest of this article. The full orbital profile of this phase is represented in Figure 2a.

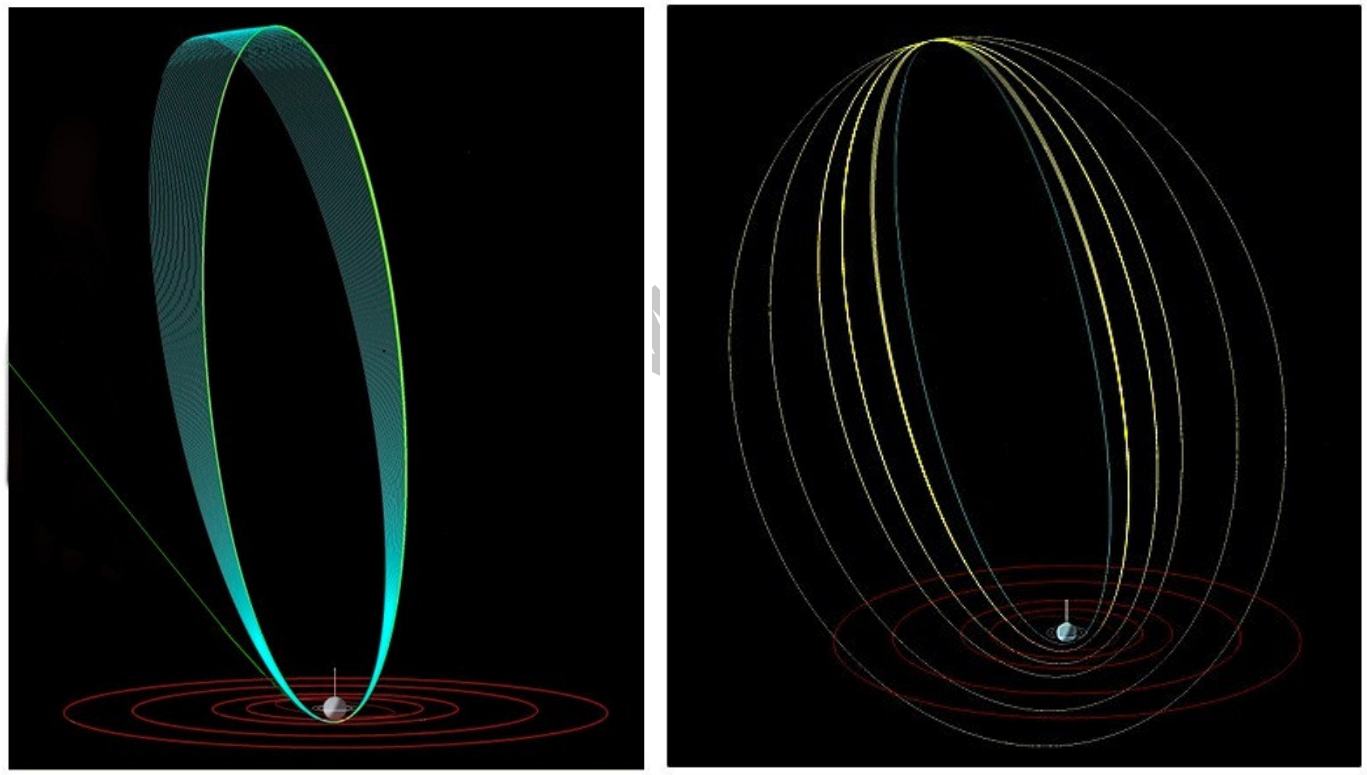

(a) Orbital profile of the Uranus Science Orbit (USO) phase

(b) Orbital profile of the Moon Tour (MT) phase

Figure 2: Spacecraft orbits for the mission's science phases. In (a) the incoming interplanetary trajectory is depicted in green and the capture orbit is depicted in yellow. The red lines depict the orbits of each of the five major moons of Uranus in both figures. In (b) The yellow lines represent the different orbits of the Moon Tour phase.

5.5.2. Moon Tour (MT)

After the completion of the USO phase, the orbiter will continue to the Moon Tour (MT) phase, which will last three years. The objective of this phase is to perform a "tour" to closely study Uranus' five largest satellites, namely Miranda, Ariel, Umbriel, Titania, and Oberon.

The MT starts with an apoapsis burn which will raise the periapsis. This orbit will make the orbiter cross the orbit of Miranda at Uranus' equatorial plane. By making this first MT orbit (MT1) resonant to Miranda, the spacecraft will perform one Miranda flyby per spacecraft orbit. After the MT1 phase is completed, another apoapsis burn will take place to raise the orbit's periapsis to get the spacecraft into its second MT orbit (MT2),

Table 11: Moon tour orbit characteristics.

Phase	Periapsis [R_U]	Apoapsis [R_U]	Eccentricity	Inclination [deg]	Period [days]
USO	1.2	60	0.96	90	20.2
MT1	1.9	60	0.9	90	20.5
MT2	3.2	60	0.9	90	21.2
MT3	4.6	60	0.8	90	23.0
MT4	8.1	60	0.7	90	23.7
MT5	11.9	60	0.6	90	25.7

which will cross Ariel's orbit at Uranus equatorial plane and will perform one Ariel flyby per spacecraft orbit. After the MT2 phase is completed, this procedure is repeated successively with Umbriel (MT3 phase), Titania (MT4 phase), and Oberon (MT5 phase). The orbital profile of the overall MT Phase is depicted in Figure 2b, the orbit characteristics of each MT orbit are summarized in Table 11, and the ΔV required for the MT phase is shown in Table 12.

The duration of each of the MT phases (MT1 to MT5) has not been fixed at the moment, since there are not sufficient scientific arguments to argue which moon should deserve more focus. Therefore, since the total duration of the MT was set to be three years, it was equally divided among the MT phases until more research can be done on this respect. For the moment, the orbit has been designed for the spacecraft to perform nine flybys per moon, completing an overall three years moon tour.

Table 12: Moon tour ΔV budget

Maneuver	ΔV [km/s]
USO to MT1	0.1
MT1 to MT2	0.14
MT2 to MT3	0.11
MT3 to MT4	0.22
MT4 to MT5	0.17
MT navigation	0.17
MT subtotal + margins*	0.96

*Margins calculated in agreement with (SRE-PA & D-TEC staff, 2011).

5.5.3. Science Operations Strategy

Given that the orbits for the USO and MT phases are highly eccentric, it will only be possible to carry out scientific measurements during specific time intervals along each orbit. For this reason, a number of science phases have been identified for each of the orbits of USO and MT. Figure 3 shows the different sections of each orbit, where point A corresponds to the moment at which the spacecraft is at a distance of 15 r_U from Uranus' center, point B is the point where the spacecraft crosses the moon plane, C is the point where the spacecraft orbit crosses the terminator, D is the point of occultation ingress, E is the point of occultation egress, and F is the point when the spacecraft reaches again a distance of 15 r_U with respect to Uranus' center.

For each of the orbit science phases different operation modes will be implemented. The operation modes are the Magnetosphere Investigation Mode (MIM), Night-side Remote Sensing mode (NRS), Day-side only Remote Sensing mode (DRS) and GRAVity measurements mode (GRAV). Table 13 shows the time spent in each of the orbit science phases for the different spacecraft orbits (USO and MT) and the corresponding modes during each phase (which can be set to operate at full or half performance during the corresponding science phase).

5.6. Ground segment

The mission operations center, located at ESOC, will monitor and control the mission. It is also responsible for generating and providing the raw data sets. ESA's ESTRACK 35 m deep space antennas will be used as the

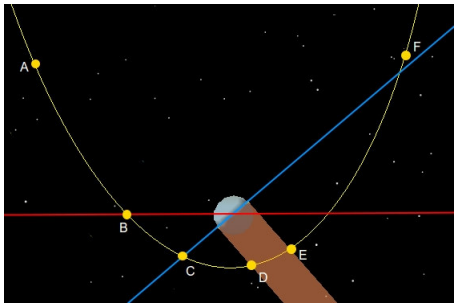

Figure 3: Schematic representation of the science phases identified for the orbits of USO and MT. The six events in the spacecraft trajectory that mark the beginning and end of a specific science phase are: A) S/C-Uranus center distance of 15 r_U before periapsis passage, B) Intersection with moons plane, C) Terminator, D) Uranus occultation ingress, E) Uranus occultation egress, F) S/C-Uranus center distance of 15 r_U after periapsis passage.

Table 13: Duration and operation mode in the science phase. The upper part of the table shows the duration of the different science phases for the USO and MT. The lower part of the table shows the performance of each operation mode, full or half performance. B-leading and B-trailing correspond to the period of time where measurements are focused on a specific moon, before and after moon flyby (B being the event marker for flyby).

Phase	A-B [hr]	B-leading [min]	B-trailing [min]	B-C [hr]	C-D [hr]	D-E [hr]	E-F [hr]	F-A [d]
USO	14.8				0.3	1	14	18.7
MT1	11	8	5	2.9	1.6	1.4	14.7	19.1
MT2	7.3	8	9	5.4	3.7	1.8	14.3	19.7
MT3		11	11	9.2	6.3	2	13.5	20.3
MT4		15	15	19.8	15.7	2.8		22.1
MT5		20	20	32.9	28.6	3.4		23
MIM	Full	Full	Full	Full	Full	Full	Full	Half
NRS	Full	Full	Full	Full	Half	Half	Half	
DRS	Full	Full	Full	Full				
GRAV		Full	Full					

Table 14: Mission ΔV budget

Maneuver	ΔV [km/s]
Interplanetary trajectory	0.21
Probe release	0.02
Uranus orbit insertion	1.01
Moon tour	0.96
Mission Total + Margin*	2.20

*Margins calculated in agreement with (SRE-PA & D-TEC staff, 2011).

main stations for tracking and receiving telemetry data from the spacecraft. Additionally, NASA's DSN can also be considered as available for specific mission operations.

The science operations center will be ESA ESAC, which supports scientific mission planning and creates pre-processed scientific data. ESAC will also be the data center for distribution, archival and similar purposes. The probe ground segment supports the operations of the probe before and after the probe science phase. The orbiter science phase will be supported by ground-based observations on Earth, and near-Earth space telescopes. The radio science data will be reduced and analyzed by instrument teams of national agencies.

5.7. End of life and planetary protection

Mission End Of Life (EOL) shall have as little impact on the engineering solution as possible. As it will be shown in Section 6.9, the mass margins, though feasible, are tight, and as such any mass penalty due to EOL shall be avoided. Spacecraft disposal is constrained by internationally ratified Planetary Protection Policy (Rummel et al., 2002). Within this framework, the Uranian system is classified as Category II. For this mission, EOL will thus be accommodated simply by shutting down all systems. Rummel et al. (2002) calls for a brief planetary protection plan. In the final observation phase the spacecraft will be in a resonance orbit with Oberon, which means the chance and impact of a collision after system shutdown must be investigated and reported as well. Possible lifetime extensions shall be studied at least one year before the officially planned mission close-out date.

6. Platform requirements and design

A preliminary space segment has been designed to analyze the capabilities required for supporting the model payload in an end-to-end system. This study lead to an estimated spacecraft dry mass of 2073 kg (including margins), and a total launch mass of 4240 kg. The spacecraft architecture is sketched in Figure 4. The vehicle is designed as a best compromise to be able to cope with the design drivers, which can be identified for this mission as follows:

- The remoteness of Uranus at a distance to Earth of 20 AU on average is a major design driver. First, it dictates the antenna design since communication data rates will be limited. Second, the low solar flux enforces the use of a Radioisotope Power Source (RPS), involving its own challenges, see also Section 7.
- It takes at least 16.45 years to reach Uranus, see Section 5. With added operations time, this leads to a very long expected mission lifetime, calling for a highly reliable space system.
- During its transfer to Uranus the spacecraft faces extreme changes of the thermal environment; on one hand, the hot thermal environment during the Venus fly-by close to the Sun, and on the other hand, the very cold environment at Uranus.

The following paragraphs give a brief overview of the spacecraft design and its subsystems meeting the requirements derived from the list above. The most important two subsystems for MUSE are discussed first, with power in Section 6.1 and communications in Section 6.2. The critical orbiter/probe interface is discussed after that in Section 6.3. The structural design is detailed in Section 6.4, which is followed by an explanation of the propulsion system in Section 6.5. The attitude and thermal control systems are discussed in Sections 6.6 and 6.7 respectively. Finally, the entry probe is treated in Section 6.8, and the chapter is concluded with an overview of the system budgets in Section 6.9.

6.1. Power

For the primary spacecraft power supply it is essential to assume that an RPS can be used. Solar power is not a feasible option because of the great distance between the Sun and Uranus. Therefore, Advanced Stirling Radioisotope Generators (ASRGs) will be used for the mission. These are preferred over RTGs because ASRGs are nearly four times as efficient (23.4 % vs 6.3 %) and have a slightly improved specific power (Abelson et al., 2005). The possibility of ESA developing this hardware will be discussed in Section 7.

A single ASRG unit will have a mass of 34 kg, providing 160 W at the beginning of life, with an annual degradation of 0.8% (Christian Erd, ESA, personal communication, August 14, 2014). The power requirements of the separate subsystems have been analyzed from their constituent parts and operational phases in order to size the power system. The resulting power budget is displayed in Table 16.

Due to the mission profile, the instruments package and the communications interface between probe and spacecraft will not operate at the same time. Thus the science phases in Uranus orbit strongly drive the system design. In these phases most of the instruments, the On-Board Data Handling (OBDH), and the Attitude and Orbit Control System (AOCS) will need to be active together. The required power at each in-orbit phase was analyzed to obtain the global power and energy requirement and a trade-off was made between the number of batteries and ASRGs. Whereas three ASRGs and 40 kg of rechargeable Lithium-ion batteries or three ASRGs would suffice to fulfill the scientific objectives, it has been chosen to use four ASRGs, providing 436 W of power after 23 years, taking into account two years of pre-launch storage, and 40 kg of Lithium batteries with a capacity of 3376 Wh after 23 years. This option ensures a full backup during peak power operations, even in case of an ASRG failure.

6.2. Communications

The single most limiting component to the effective science return in a mission to distant regions of the Solar System is the achievable transmission rate of the acquired data. Telemetry rates of any spacecraft are essentially constrained by three characteristics: distance, power, and antenna gain. In this case, the communications distance is given by the relative distances of Uranus to the Earth of about 18.4 ± 1 AU in perihelion and 20.1 ± 1 AU in aphelion. Power consumption of the transmitter is severely limited as well and cannot be expected to exceed more than 50 W to 100 W for practical reasons, as the whole spacecraft has to be driven by a number of RPSs. As for the antenna gain, it is made up of two properties: the diameter of the dish and the operating frequency. The former is constrained by the payload fairing of the spacecraft and unlikely to exceed more than approximately 5 m (Ariane 5). The latter is limited to the available hardware for both space applications and is also problematic

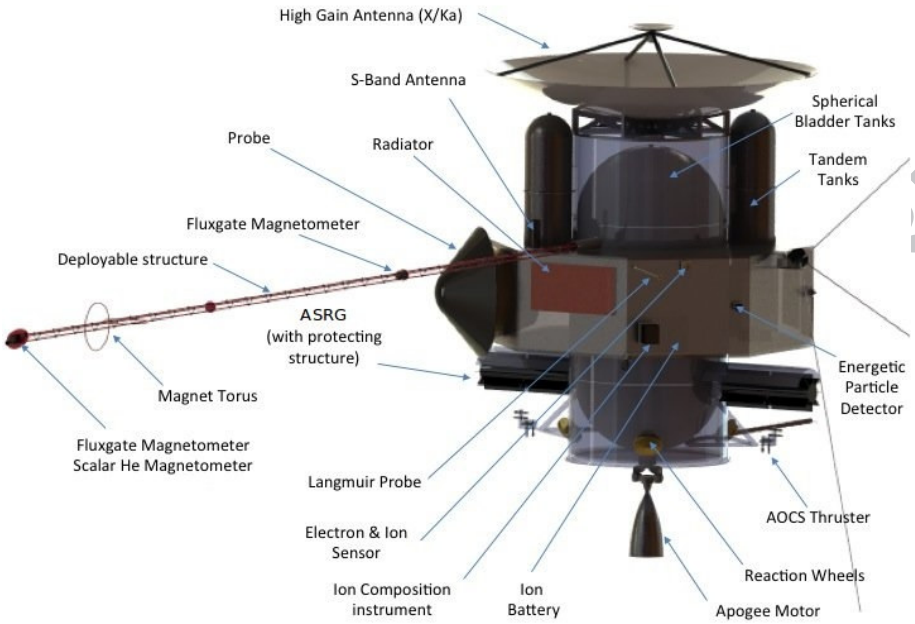

(a) Front side.

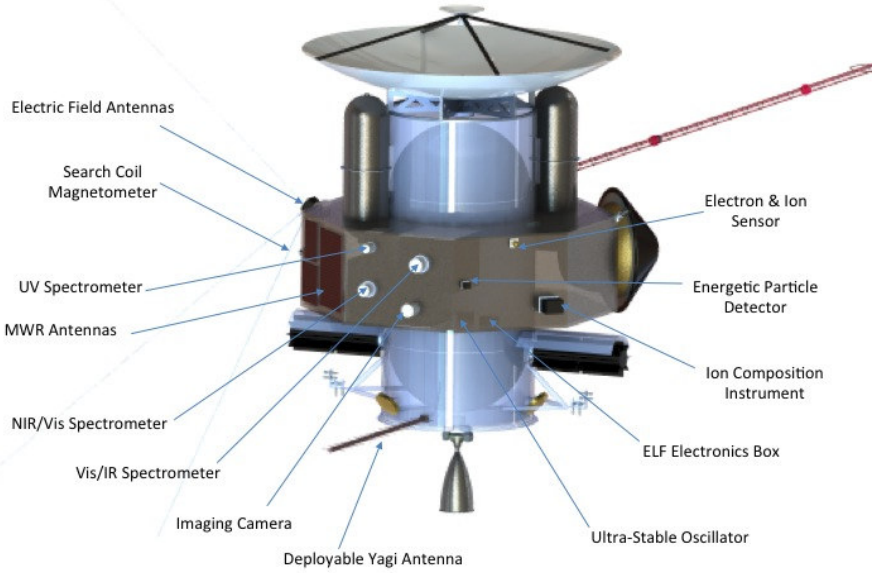

(b) Back side.

Figure 4: Spacecraft concept demonstrating the capability to support all instruments.

towards higher frequencies, as absorption and scattering due to local line-of-sight atmospheric water content will increase noise and signal attenuation of another ~ 0.1 dB/km in Ka- compared to X-band (ITU, 2013). Without considering any forward error-correction, such as low-density parity-check or turbo codes, available downlink telemetry rates can be estimated to be ~ 3 kbps, assuming that all data are transmitted in binary phase shift keying from a 4 m dish at 8 GHz with an RF output power of 25 W, given an expected bit error probability of 10^{-3} and a pointing loss of a no more than 1 dB.

6.3. Orbiter/Probe interface

The telemetry of the PEP is to be split in two phases. During the coasting phase, periodically a minimum amount of housekeeping data is needed in order to monitor the probe systems status. During entry and descent, real-time telemetry is required to relay flight and instrumental measurements data. Considering the atmospheric attenuation effects and the desired target depth of 100 bars, a carrier link frequency in the lower portion of the UHF band is chosen. This is in accordance with the ESA PEP study (Falkner et al., 2010), where a frequency of 400 MHz at 100 W RF output power and an expected maximum attenuation of 15 dB is assumed. The antenna on the spacecraft is preferably a deployable axial-mode helical or circular polarized cross-yagi design given the operating frequency and achievable gain over an omnidirectional antenna. Adopting the analysis and design presented in Falkner et al. (2010), the probe shall be equipped with two antennas. A patch antenna on the back of the protective cover shall be employed during the coasting phase for low-power, low-rate housekeeping telemetry, while a deployable omnidirectional helix antenna is to be used during the descent phase for high-rate data telemetry after the cover is jettisoned.

6.4. Structural Configuration and Mechanism

The spacecraft structure aims at an optimal payload accommodation while minimizing structural mass and reducing its impact on other subsystems. A central tube configuration is used as the primary structure. It supports the two stacked, spherical propellant tanks, and its outer diameter is defined by the launch adapter ($d_{out} = 1660$ mm). The pressurant tanks are attached to the outside of the tube. A ground plate provides additional shear stiffness against bending forces during the launch and the firing of the main engine. A supporting aluminum alloy truss structure, which also holds the High Gain Antenna (HGA), forms the upper shear stiffness-providing structure. The central tube serves additionally as a secondary structure and provides attachments for subsystems (such as the ASRGs, reaction wheels, attitude control thrusters, etc.). The technology used for the structural configuration is flight proven and has a TRL of 9. The spacecraft has an overall dimension of 4.4 m $\times$ 4.5 m (diameter $\times$ height in undeployed configuration, height measured from launch adapter).

The payload is arranged on the faces of an octagonal support structure, which is itself attached to the central tube. This configuration results in minimal interference between the antenna and instruments. The arrangement also enables synchronous planet-pointing without changing the attitude of the spacecraft.

The accommodation of the two ASRGs below this ring minimizes their thermal and radiation impact on other spacecraft subsystems and/or payload. The payload accommodation ring also provides further shielding.

Indispensable mechanisms are deployable booms for the Langmuir probes, antennas, and for the magnetometers; each of them is driven by a spring mechanism which is initiated by a pyrotechnic device (high reliability, TRL=9). For the separation of the atmospheric probe the release mechanism of Cassini shall be used because of flight-heritage and probe spin-up design (TRL=9).

6.5. Propulsion System

The driving parameters of the propulsion system are the required ΔV for the orbital maneuvers and attitude control sequences, $\Delta V = 2200$ m/s (see Table 14), as well as the required thrust F. These parameters lead to the following proposed propulsion system configuration.

A bi-propellant propulsion system with the highly stable and storable Monomethylhydrazine and Mixed Oxides of Nitrogen (MMH/MON) propellant combination is used. The engine is integrated on a gimbal in order to cope with drifts of the vehicle's center of mass. Spherical tanks are used for both the fuel and the oxidizer (in bladder tank configuration). In addition, two cylindrical tanks, made of a light titanium alloy, such as $TiAl_6V_4$, are used for the helium pressurant. This configuration minimizes system mass and optimizes the propellant feed. Full single redundancy shall be provided for the entire feed system.

6.6. Attitude and Orbit Control System (AOCS)

The driving parameters of the AOCS are the required angular acceleration of the spacecraft and the needed pointing accuracy. Both are driven by the demands of specific experiments, such as optical remote sensing and gravity measurements, and of the communications payload in general (the accuracy and stability needed to point the antenna at Earth for downlink).

Three star trackers (double redundancy in each axis), three fine Sun sensors (a special design taking into account the long Uranus-Sun distance), six coarse sun sensors (TRL 9, equipped for safe–mode sun acquisition and operations in the inner Solar System) and two inertial measurement units shall provide the required attitude determination with the required accuracy. The AOCS controller realizes the commanded state using four reaction wheels (single redundancy in each axis in tetrahedral configuration). The OBDH defines the operational AOCS mode and therefore the required angular position. It also determines the momentum saturation of the wheels and determines if wheel unloading is required, which 24 bi-propellant thrusters will accomplish (double redundancy in each axis). The technology used for the AOCS configuration is flight proven and is qualified with TRL 9, excluding the fine sun-sensors and thrusters.

6.7. Thermal Control System (TCS)

The TCS provides a stable thermal environment of around 280 K inside the spacecraft. The HGA, painted with white epoxy, shields the spacecraft in the inner Solar System and especially during the Venus flyby, while a Multi Layer Insulation (MLI) cover improves thermal stability. According to the preliminary design, no additional internal heaters have to be foreseen; radiators on the spacecraft surface give the possibility to radiate excess power produced by the ASRGs. The internal thermal circuit will consist of two toroidal heat pipes for the payload-section and spiral-shaped ones for the cylinder section to distribute the generated heat. Louvers have been avoided in order to increase reliability of the TCS.

The driving case occurs during communications at Uranus according to the power output of the antenna. For high internal power output scenarios, the spacecraft temperature will be increased by 15 K in the worst case. Furthermore, the thermal losses of the ASRGs can provide additional energy if the internal design makes it necessary. The TCS has been designed for a 25 year mission but allows for three to four additional years due to temperature margins.

6.8. Uranus Entry Probe

The major design constraint of the entry probe is its mass, which shall be minimized and shall not exceed 312 kg, based on the mass budget provided by Falkner et al. (2010). Besides the science payload identified in Table 4, and the basic subsystems, the probe shall accommodate flight instrumentation and a parachute system, all placed in a descent module, which in turn is covered by a front shield and back cover. The front shield and back cover shall survive the thermal environment during coasting and then during entry. After entry, the front shield and back cover are released, the parachute is deployed and the descent module will perform scientific measurements during its descent in Uranus' atmosphere down to 100 bars (refer to Section 3.1 for the requirement rationale).Due to this requirement, the structural mass is expected to be a substantial percentage of the overall mass budget. During its descent, a relay link shall be available with the orbiter to transmit the collected data, with the specifications mentioned in Section 6.3.

6.9. System budgets

The dry mass has been estimated to be 2073 kg (see Table 15), placing it between Cassini (2558 kg) and Galileo (1782 kg). This renders the spacecraft one of the heaviest deep-space probes ever, underlining that MUSE will truly be a flagship endeavor. The estimation procedure was based on existing hardware characteristics where possible, and parametric estimation methods where data is unobtainable.

ESA's Margin Philosophy for Science Assessment Studies has been strictly followed to come up with a conservative mass estimate on sub-system and system level, and also for computing the ΔV (SRE-PA & D-TEC staff, 2011). With margins, a total launch mass of 4240.1 kg is estimated, leaving a 2% margin for the launch. This figure is comparable to other assessment studies, such as one of the JUICE spacecraft designs (Dougherty et al., 2011).

The mass budget can be sensitive to any design changes or unexpected issues. This must be especially considered with the introduction of new technologies such as the ASRGs. Even with the considerable margins which have been applied to the estimates where applicable, budget overruns cannot be avoided with all certainty. Concerning this it must be noted that an Ariane 5 ECA launch vehicle has been assumed, while the Ariane 5 ME program has been kept in motion at ESA's Ministerial Council in 2012. This means that an improvement of

up to 30% in launch mass can be expected, thus most likely increasing the margins considerably by the time of launch.

Table 15: Mass budget for MUSE including design maturity and system margins. Note that differences with respect to Table 7 may occur due to applied design maturity margins.

Subsystem	Mass (including margin) [kg]
Probe	312
Scientific payload	89.5
VINIRS	11
IRS	15
UVIS	4
RPW	6
MAG (incl. boom)	11
TELFA	2
ICI	5.7
EIS	3.6
EPD	3
NAC	8.6
WAC	4
RSE*	
MWR	14
DC	1.6
Radioisotope power system, incl. harness	285.1
Structure	330
Communications	154.2
OBDH	51.5
AOCS	83.5
Thermal control	66
Propulsion	200.7
Launcher adapter	155.0
Nominal dry spacecraft mass	1727.5
System level margin (20%)	345.5
Total dry mass	2073
Propellant mass (incl. 309 kg for AOCS)	2167.1
Total launch mass	4240.1
Ariane 5 ECA launch vehicle performance	4300
Excess launch capability (2%)	59.9

* RSE mass budget is included in the communications system budget.

The power budget for the most-demanding operational cases is shown in Table 16. All powers include margins on the power source (included average degradation per years) and on each individual instrument. Because of the important peak power during the science phase, an extra lithium battery of 40 kg is used to provide 3375 Wh and then cover all particular needs. All operational scenarios have been studied to ensure that the power supply by the ASRG and Lithium battery is sufficient to enable science operations and offer a sufficient back up in case of an ASRG failure.

Table 16: Power budget for MUSE including design maturity margins for the defining operational cases. The extra energy is needed to support operations in the peak power case for an extended observational period.

Subsystem	Downlink case [W]	Max instrument operations [W]
Platform	260.4	200.4
Communications	93.9	33.9
AOCS	116.1	116.1
Propulsion	0	0
OBDH	50.4	50.4
Payload	39	136
VINIRS & UVIS	2	52
IRS	2	33
RPW	7	7
MAG	8	8
TELFA	2	5
ICI	5.6	5.6
EIS	3.8	3.8
EPD	4.6	4.6
NAC & WAC	2	15
MWR	2	2
Total need	299.4	336.4
ASRG provision	319.45	327.26
Extra energy need [Wh]	0	2570

7. Programmatics and public outreach

Within the ESA programmatic framework, this mission would classify as an L-class mission. Although no reliable cost-estimates have been established, meeting the common cost cap (about FY13 M€900 to M€1000) for this class will be a big programmatic challenge. While not essential for the realization of MUSE, decision makers might consider international cooperation. It should be pointed out that the mission provides ample attractive opportunities for potential partners, for example, the science-crucial probe could be developed together with another agency.

Technologically, the mission presents several important risks, but none of them have been identified as insurmountable, for the short to mid-term (see Section 6). The key technology that this mission demands is a RPS, see also Section 6.1. Arridge et al. (2011) already analyzed this issue, and concluded that it is within European reach to build a suitable device by 2021. As this mission would be due for launch in 2026 only, this even leaves 13 years of development time from the date of writing. With backup systems available in the United States and possibly Russia, this technological risk is within acceptable boundaries. Remaining subsystems will not require major modifications from existing designs, and present a high TRL throughout.

The second issue of concern is the long lifetime the mission would need to endure. For this reason, MUSE will be built based on components with very strong heritage. Considerable experience with deep-space missions was gained in the past by both, ESA and NASA. The Cassini spacecraft provides an example of a very long lasting outer-planet mission. Only an evolutionary improvement over past missions will be required to achieve acceptable risk figures, and these mitigation measures are within the reach of such a program. Thorough quality assurance and a testing strategy comparable to current procedures will enable the development of a successful mission with these high reliability requirements.

Apart from a significant scientific return, MUSE is expected to deliver in terms of public attention and media return. MUSE would be the first mission since Voyager 2 to explore Uranus, strongly appealing to human interest in general. Furthermore, the cooperation between national agencies will help to organize activities around major mission milestones. Due to the long duration of the overall mission, there is opportunity to involve new generations of students and get them excited about space research.

MUSE will be a particularly prestigious and valuable mission, because it will be the first orbiter of an ice giant to conduct the first detailed study of the Uranian system, perform the first detailed investigation of Uranus' atmosphere using a probe, and conduct the first detailed study of Uranus' magnetic field.

8. Conclusion

The planet Uranus, as one of two ice giants in the Solar System, can be understood as an archetype for this type of planets in exoplanetary systems. Therefore, by visiting Uranus with a robotic spacecraft, knowledge will be increased not only of the formation and evolution of the Uranian system, but ice giant exoplanets and planetary system formation in general.

This paper presented the process of generating the conceptual design for a mission to the Uranian system. The key science questions to be addressed were identified to be those related to Uranus' atmosphere and the interior of the planet. Investigations of the magnetosphere and the Uranian system, although highly interesting in their own right, are more specific to the planet itself and will provide less knowledge on ice giants in general, making them of lower importance for these mission goals. The science questions that the mission is to address were defined, their relative importance determined, and instruments were selected, capable of performing the measurements required for answering these questions. A comprehensive trade-off was performed, considering several types of missions, for which an instrument suite was defined and its capability of answering the science questions in each configuration analyzed. The trade-off was performed based on engineering and science criteria separately, the results of which were then combined to generate an optimality envelope of mission types as a function of the relative science/engineering importance in the decision process. The results showed that, for a typical science weight of 70% (*i. e.*, a mission driven by the science return but constrained by engineering considerations), an orbiter with a single atmospheric entry probe and flybys of the main satellites in the system would be best suited to answer the science questions that were generated.

The mission and system design for this concept was performed, resulting in a launch in 2026 and an arrival at Uranus in 2044. A number of alternative launch options were also identified, giving the option for descoping or enhancing the mission. Following an initial Uranus science orbit, the spacecraft will perform close flybys of each of its five largest moons, providing a comprehensive science return. The system design of the spacecraft is strongly driven by the large distance from the Sun where it is to operate, requiring the use of a radioactive power source and a large antenna dish. Also, the long mission lifetime imposes stringent constraints on the reliability of the spacecraft subsystems.

This mission to the Uranian system will be a major step in understanding processes occurring in ice giants, by means of both, remote sensing and actual in-situ measurements. As such, it is a crucial step in balancing knowledge of planetary systems; improving understanding of ice giants to a level more comparable to that of rocky planets and gas giants, furthering the scientific understanding of not only the Solar System, but exoplanetary systems throughout the universe.

Acknowledgements

The authors acknowledge funding from ESA and the Austrian Research Promotion Agency during the Alpbach Summer School 2012 "Exploration of the icy planets and their systems" and the following one-week meeting in Graz. This study benefited from the work of 45 other students during the above mentioned summer school. The authors also would like to thank all the tutors and organisers of the summer school for their support.

References

Abelson, R. D., Balint, T., Coste, K., Elliott, J., Randolph, J., Schmidt, G., Schriener, T., Shirley, J., & Spilker, T. (2005). Expanding frontiers with standard radioisotope power systems. Tech. Rep. JPL D-28902 PP-266 0332, NASA.
URL `http://solarsystem.nasa.gov/scitech/display.cfm?ST_ID=705`

Airy, G. B. (1847). Account of some circumstances historically connected with the discovery of the planet exterior to Uranus. *Astr. Nachr.; AN*, *25*(10), 131–148. DOI:10.1002/asna.18470251002.

Alibert, Y., Mordasini, C., Benz, W., & Winisdoerffer, C. (2005). Models of giant planet formation with migration and disc evolution. *Astron. Astrophys.*, *434*(1), 343–353. DOI:10.1051/0004-6361:20042032.

Arridge, C., Agnor, C., André, N., Baines, K., Fletcher, L., Gautier, D., Hofstadter, M., Jones, G., Lamy, L., Langevin, Y., et al. (2011). Uranus Pathfinder: exploring the origins and evolution of Ice Giant planets. *Exp. Astron.*, *33*(2-3), 753–791. DOI:10.1007/s10686-011-9251-4.

Baines, K. (1995). The abundances of methane and ortho/para hydrogen on Uranus and Neptune: Implications of New Laboratory 4-0 H_2 quadrupole line parameters. *Icarus*, *114*(2), 328–340. DOI:10.1006/icar.1995.1065.

Baines, K. H., & Bergstralh, J. T. (1986). The structure of the Uranian atmosphere: Constraints from the geometric albedo spectrum and H_2 and CH_4 line profiles. *Icarus*, *65*(2-3), 406–441. DOI:10.1016/0019-1035(86)90146-6.

Bignami, G., Cargill, P., Schutz, B., & Turon, C. (2005). Cosmic vision: Space science for Europe 2015-2025.
URL `http://www.esa.int/esapub/br/br247/br247.pdf`

Biscani, F., Izzo, D., & Yam, C. H. (2010). A global optimisation toolbox for massively parallel engineering optimisation. ArXiv preprint arXiv:1004.3824.

Bodenheimer, P., & Lin, D. (2002). Implications of extrasolar planets for understanding planet formation. *Annu. Rev. Earth Planet. Sci.*, *30*, 113–148.

Bond, P. (2012). *Uranus*, (p. 297). Wiley-Blackwell, 1st ed.

Boss, A. P. (1997). Giant planet formation by gravitational instability. *Science*, *276*(5320), 1836–1839. DOI:10.1126/science.276.5320.1836.

Boss, A. P. (2002). Formation of gas and ice giant planets. *Earth Planet. Sci. Lett.*, *202*(3-4), 513–523. DOI:10.1016/s0012-821x(02)00808-7.

Broadfoot, A., Herbert, F., & Holberg, J. (1986). Ultraviolet spectrometer observations of Uranus. *Science*, *233*(4759), 74–79. DOI:10.1126/science.233.4759.74.

Burch, J. L., Goldstein, R., Cravens, T. E., Gibson, W. C., Lundin, R. N., Pollock, C. J., Winningham, J. D., & Young, D. T. (2006). RPC-IES: The Ion and Electron Sensor (IES) of the Rosetta Plasma Consortium (RPC). *Space Sci. Rev.*, *128*(1-4), 697–712. DOI:10.1007/s11214-006-9002-4.

Canup, R., & Ward, W. (2000). A possible impact origin of the Uranian satellite system. In *Bull. Am. Astron. Soc.*, vol. 32, (p. 1105).

Cheng, A. F. (1987). Proton and oxygen plasmas at Uranus. *J. Geophys. Res.*, *92*(A13), 15309. DOI:10.1029/ja092ia13p15309.

Cody, A., & Stevenson, D. (2005). Constraining the gravitational energies of Uranus and Neptune from interior models: Implications for formation. In *Bull. Am. Astron. Soc.*, vol. 37, (p. 677).

Conrath, B., Gautier, D., Hanel, R., Lindal, G., & Marten, A. (1987). The helium abundance of Uranus from Voyager measurements. *J. Geophys. Res.*, *92*(A13), 15003. DOI:10.1029/ja092ia13p15003.

Cowley, S. W. H. (2013). Response of Uranus' auroras to solar wind compressions at equinox. *J. Geophys. Res. Space Physics*, *118*(6), 2897–2902. DOI:10.1002/jgra.50323.

De Pater, I., Romani, P. N., & Atreya, S. K. (1989). Uranus deep atmosphere revealed. *Icarus*, *82*(2), 288–313. DOI:10.1016/0019-1035(89)90040-7.

Dougherty, M., Grasset, O., Bunce, E., Coustenis, A., Blanc, M., Coates, A., Coradini, A., Drossart, P., Fletcher, L., Hussmann, H., Jaumann, R., Krupp, N., Prieto-Ballesteros, O., Tortora, P., Tosi, F., van Hoolst, T., Titov, D., Erd, C., Wielders, A., Altobelli, N., Favata, F., Escoubert, P., et al. (2011). JUICE yellow book: Exploring the emergence of habitable worlds around gas giants.
URL `http://sci.esa.int/juice/49837-juice-assessment-study-report-yellow-book/#`

Dougherty, M., Kellock, S., Southwood, D., Balogh, A., Smith, E., Tsurutani, B., Gerlach, B., Glassmeier, K.-H., Gleim, F., Russell, C., et al. (2004). The Cassini magnetic field investigation: Orbiter in situ investigations. In C. Russel (Ed.) *The Cassini-Huygens mission*, vol. 2, (pp. 331–383). Springer.

Duev, D., Molera-Calvés, G., Pogrebenko, S., Gurvits, L., Cimó, G., & Bocanegra-Bahamón, T. (2012). Spacecraft VLBI and Doppler tracking: algorithms and implementation. *Astron. Astrophys.*, *541*, A43. DOI:10.1051/0004-6361/201218885.

Duncan, M. J., & Lissauer, J. J. (1997). Orbital stability of the Uranian satellite system. *Icarus*, *125*(1), 1–12. DOI:10.1006/icar.1996.5568.

England, C. (2003). Are there oceans under the ice of small Saturnian and Uranian moons? In *Bull. Am. Astron. Soc.*, vol. 35, (p. 939).

ESA (2013). Cosmic vision: White papers submitted in response to ESA's call for science themes for the L2 and L3 missions. Booklet.
URL `http://sci.esa.int/cosmic-vision/52030-white-papers-submitted-in-response-to-esas-call-for-science-themes-for-the-l2-and-l3-missions/`

Esposito, L., Brahic, A., Burns, J., & Marouf, E. (1991). Particle properties and processes in Uranus' rings. In J. Bergstralh, E. D. Miner, & M. Matthews (Eds.) *Uranus*, vol. 1, (pp. 410–465). University of Arizona Press.

Falkner, P., Geelen, K., Rebuffat, D., Larranaga, J., Romstedt, J., et al. (2010). CDF study report: PEP (SYN) Planetary Exploration Probe Synthesis. Tech. Rep. CDF-106(C), European Space Agency (ESA). Provided by ESA.

Flasar, F. M., Conrath, B. J., Gierasch, P. J., & Pirraglia, J. A. (1987). Voyager infrared observations of Uranus' atmosphere: Thermal structure and dynamics. *J. Geophys. Res.*, *92*(A13), 15011. DOI:10.1029/ja092ia13p15011.

Fortney, J. J., Ikoma, M., Nettelmann, N., Guillot, T., & Marley, M. S. (2011). Self-consistent model atmospheres and the cooling of the Solar System's giant planets. *Astrophys. J.*, *729*(1), 32. DOI:10.1088/0004-637x/729/1/32.

French, R. G., Nicholson, P. D., Porco, C. C., & Marouf, E. A. (1991). Dynamics and structure of the Uranian rings. In J. Bergstralh, E. D. Miner, & M. Matthews (Eds.) *Uranus*, vol. 1, (pp. 327–409). University of Arizona Press.

Guillot, T. (2005). The interiors of giant planets: Models and outstanding questions. *Annu. Rev. Earth Planet. Sci.*, *33*(1), 493–530. DOI:10.1146/annurev.earth.32.101802.120325.

Guillot, T., & Gautier, D. (2007). Giant planets. In G. Schubert (Ed.) *Treatise on Geophysics: Planets and moons*, vol. 10, (pp. 439 – 464). Elsevier.

Gurnett, D. A., Kurth, W., Scarf, F., Burns, J., Cuzzi, J., & Grün, E. (1987). Micron-sized particle impacts detected near Uranus by the Voyager 2 plasma wave instrument. *J. Geophys. Res.*, *92*(A13), 14959. DOI:10.1029/ja092ia13p14959.

Hanel, R., Conrath, B., Flasar, F. M., Kunde, V., Maguire, W., Pearl, J., Pirraglia, J., Samuelson, R., Cruikshank, D., Gautier, D., et al. (1986). Infrared observations of the Uranian system. *Science*, *233*(4759), 70–74. DOI:10.1126/science.233.4759.70.

Hubbard, W. (2010). Ice Giants Decadal Study. NASA Planetary Science Decadal Survey Mission Concept Study Final Report.
URL `http://www.nap.edu/reports/13117/App\%20G\%2023_Uranus_Orbiter_and_Probe.pdf`

Hubbard, W., & Marley, M. S. (1989). Optimized Jupiter, Saturn, and Uranus interior models. *Icarus*, *78*(1), 102–118. DOI:10.1016/0019-1035(89)90072-9.

Hubickyj, O., Bodenheimer, P., & Lissauer, J. (2005). Accretion of the gaseous envelope of Jupiter around a 5–10 Earth-mass core. *Icarus*, *179*(2), 415–431. DOI:10.1016/j.icarus.2005.06.021.

Hussmann, H., Sohl, F., & Spohn, T. (2006). Subsurface oceans and deep interiors of medium-sized outer planet satellites and large trans-Neptunian objects. *Icarus*, *185*(1), 258–273. DOI:10.1016/j.icarus.2006.06.005.

Irwin, P. (2009). *Giant planets of our solar system*, (pp. 121–127). Springer, 2nd ed.

ITU (2013). Attenuation by atmospheric gases. Recommendation ITU-R P.676-10, International Telecommunication Union.
URL `http://www.itu.int/dms_pubrec/itu-r/rec/p/R-REC-P.676-10-201309-I!!PDF-E.pdf`

Johnson, T., Yeates, C., & Young, R. (1992). Space science reviews volume on Galileo mission overview. *Space Sci. Rev.*, *60*(1-4). DOI:10.1007/bf00216848.

Kaiser, M. L., Desch, M. D., & Curtis, S. A. (1987). The sources of Uranus' dominant nightside radio emissions. *J. Geophys. Res.*, *92*(A13), 15169. DOI:10.1029/ja092ia13p15169.

Karkoschka, E. (2001). Comprehensive photometry of the rings and 16 satellites of Uranus with the Hubble Space Telescope (HST). *Icarus*, *151*(1), 51–68. DOI:10.1006/icar.2001.6596.

Lamy, L., Prangé, R., Hansen, K., Clarke, J., Zarka, P., Cecconi, B., Aboudarham, J., André, N., Branduardi-Raymont, G., Gladstone, R., et al. (2012). Earth-based detection of Uranus' aurorae. *Geophys. Res. Lett.*, *39*(7). DOI:10.1029/2012gl051312.

Levison, H. (2001). Remarks on modeling the formation of Uranus and Neptune. *Icarus*, *153*(1), 224–228. DOI:10.1006/icar.2001.6672.

Lindal, G. F., Lyons, J. R., Sweetnam, D. N., Eshleman, V. R., Hinson, D. P., & Tyler, G. L. (1987). The atmosphere of Uranus: Results of radio occultation measurements with Voyager 2. *J. Geophys. Res.*, *92*(A13), 14987. DOI:10.1029/ja092ia13p14987.

Livi, S., McNutt, R., Andrews, G., Keath, E., Mitchell, D., & Ho, G. (2003). The Energetic Particles Spectrometers (EPS) on MESSENGER and New Horizons. In *AIP Conference Proceedings*, (pp. 838–841).

Lunine, J. I. (1993). The atmospheres of Uranus and Neptune. *Annu. Rev. Astron. Astrophys.*, *31*(1), 217–263. DOI:10.1146/annurev.astro.31.1.217.

Matson, D. L., Spilker, L. J., & Lebreton, J.-P. (2003). The Cassini/Huygens mission to the Saturnian system. In *The Cassini-Huygens mission*, vol. 2, (pp. 1–58). Springer.

Mauk, B. H., Krimigis, S. M., Keath, E. P., Cheng, A. F., Armstrong, T. P., Lanzerotti, L. J., Gloeckler, G., & Hamilton, D. C. (1987). The hot plasma and radiation environment of the Uranian magnetosphere. *J. Geophys. Res.*, *92*(A13), 15283. DOI:10.1029/ja092ia13p15283.

Mayer, L. (2002). Formation of giant planets by fragmentation of protoplanetary disks. *Science*, *298*(5599), 1756–1759. DOI:10.1126/science.1077635.

McNutt, R. L., Livi, S. A., Gurnee, R. S., Hill, M. E., Cooper, K. A., Andrews, G. B., Keath, E. P., Krimigis, S. M., Mitchell, D. G., Tossman, B., et al. (2009). The Pluto Energetic Particle Spectrometer Science Investigation (PEPSSI) on the New Horizons mission. *Space Sci. Rev.*, *145*(3-4), 381–381. DOI:10.1007/s11214-009-9534-5.

McNutt, R. L., Selesnick, R. S., & Richardson, J. D. (1987). Low-energy plasma observations in the magnetosphere of Uranus. *J. Geophys. Res.*, *92*(A5), 4399. DOI:10.1029/ja092ia05p04399.

Miner, E. D. (1990). *Uranus: The planet, rings and satellites*. Wiley, 2nd ed.

Mizuno, H. (1980). Formation of the Giant Planets. *Progr. Theoret. Phys.*, *64*(2), 544–557. DOI:10.1143/ptp.64.544.

Neckel, H., & Labs, D. (1994). Solar limb darkening 1986–1990 (λλ303 to 1099 nm). *Sol. Phys.*, *153*(1-2), 91–114. DOI:10.1007/bf00712494.

Ness, N. F., Acuna, M. H., Behannon, K. W., Burlaga, L. F., Connerney, J. E. P., Lepping, R. P., & Neubauer, F. M. (1986). Magnetic fields at Uranus. *Science*, *233*(4759), 85–89. DOI:10.1126/science.233.4759.85.

Nettelmann, N., Helled, R., Fortney, J., & Redmer, R. (2013). New indication for a dichotomy in the interior structure of Uranus and Neptune from the application of modified shape and rotation data. *Planet. Space Sci.*, *77*, 143–151. DOI:10.1016/j.pss.2012.06.019.

Nilsson, H., Lundin, R., Lundin, K., Barabash, S., Borg, H., Norberg, O., Fedorov, A., Sauvaud, J.-A., Koskinen, H., Kallio, E., et al. (2006). RPC-ICA: The Ion Composition Analyzer (ICA) of the Rosetta Plasma Consortium (RPC). *Space Sci. Rev.*, *128*(1-4), 671–695. DOI:10.1007/s11214-006-9031-z.

O'Brien, R., Ambrosi, R., Bannister, N., Howe, S., & Atkinson, H. (2008). Safe radioisotope thermoelectric generators and heat sources for space applications. *J. Nucl. Mater.*, *377*(3), 506–521. DOI:10.1016/j.jnucmat.2008.04.009.

Peterson, C., Cutts, J., Balint, T., & Hall, J. B. (2008). Rapid cost assessment of space mission concepts through application of complexity-based cost indices. In *Aerospace Conference, 2008 IEEE*, (pp. 1–8). IEEE.

Pingree, P., Janssen, M., Oswald, J., Brown, S., Chen, J., Hurst, K., Kitiyakara, A., Maiwald, F., & Smith, S. (2008). Microwave radiometers from 0.6 to 22 GHz for Juno, a polar orbiter around Jupiter. In *Aerospace Conference, 2008 IEEE*, (pp. 1–15).

Podolak, M., Hubbard, W. B., & Stevenson, D. J. (1991). Models of Uranus' interior and magnetic field. In J. Bergstralh, E. D. Miner, & M. Matthews (Eds.) *Uranus*, vol. 1, (pp. 29–61). University of Arizona Press.

Pollack, J. (1996). Formation of the giant planets by concurrent accretion of solids and gas. *Icarus*, *124*(1), 62–85. DOI:10.1006/icar.1996.0190.

Ragent, B., Privette, C., Avrin, P., Waring, J., Carlston, C., Knight, T., & Martin, J. (1992). Galileo probe nephelometer experiment. *Space Sci. Rev.*, *60*(1-4). DOI:10.1007/bf00216854.

Rummel, J., Stabekis, P., Devincenzi, D., & Barengoltz, J. (2002). COSPAR's planetary protection policy: A consolidated draft. *Adv. Space Res.*, *30*(6), 1567–1571. DOI:10.1016/s0273-1177(02)00479-9.

Saur, J., Neubauer, F. M., & Glassmeier, K.-H. (2009). Induced magnetic fields in Solar System bodies. *Space Sci. Rev.*, *152*(1-4), 391–421. DOI:10.1007/s11214-009-9581-y.

Schneider, J., Dedieu, C., Le Sidaner, P., Savalle, R., & Zolotukhin, I. (2011). Defining and cataloging exoplanets: the exoplanet.eu database. *Astron. Astrophys.*, *532*, A79. DOI:10.1051/0004-6361/201116713.

Selesnick, R. S., & Richardson, J. D. (1986). Plasmasphere formation in arbitrarily oriented magnetospheres. *Geophys. Res. Lett.*, *13*(7), 624–627. DOI:10.1029/gl013i007p00624.

Showalter, M. R. (2006). The second ring-moon system of Uranus: Discovery and dynamics. *Science*, *311*(5763), 973–977. DOI:10.1126/science.1122882.

Simões, F., Pfaff, R., Hamelin, M., Klenzing, J., Freudenreich, H., Béghin, C., Berthelier, J., Bromund, K., Grard, R., Lebreton, J., et al. (2012). Using Schumann resonance measurements for constraining the water abundance on the giant planets – Implications for the Solar System's formation. *Astrophys. J.*, *750*(1), 85. DOI:10.1088/0004-637x/750/1/85.

Slattery, W. L., Benz, W., & Cameron, A. (1992). Giant impacts on a primitive Uranus. *Icarus*, *99*(1), 167–174. DOI:10.1016/0019-1035(92)90180-f.

Smith, B. A., Soderblom, L., Beebe, R., Bliss, D., Boyce, J., Brahic, A., Briggs, G., Brown, R., Collins, S., Cook, A., et al. (1986). Voyager 2 in the Uranian system: Imaging science results. *Science*, *233*(4759), 43–64. DOI:10.1126/science.233.4759.43.

Squyres, S., et al. (2011). Vision and voyages for planetary science in the decade 2013–2022. Committee on the Planetary Science Decadal Survey; National Research Council.
URL `http://solarsystem.nasa.gov/docs/Vision_and_Voyages-FINAL.pdf`

Srama, R., Ahrens, T., Altobelli, N., Auer, S., Bradley, J., Burton, M., Dikarev, V., Economou, T., Fechtig, H., Görlich, M., et al. (2004). The Cassini Cosmic Dust Analyzer (CDA). *Space Sci. Rev.*, *114*(1-4), 465–518. DOI:10.1007/s11214-004-1435-z.

SRE-PA & D-TEC staff (2011). Margin philosophy for science assessment studies. Tech. Rep. SCI-PA/2007/022/, European Space Agency (ESA). Provided by ESA.

Sromovsky, L. (2000). Ground-based observations of cloud features on Uranus. *Icarus*, *146*(1), 307–311. DOI:10.1006/icar.2000.6434.

Sromovsky, L., & Fry, P. (2008). The methane abundance and structure of Uranus' cloud bands inferred from spatially resolved 2006 Keck grism spectra. *Icarus*, *193*(1), 252–266. DOI:10.1016/j.icarus.2007.08.037.

Stevenson, D. (2004). Formation of giant planets. *American Institute of Physics Conference Proceedings*, *173*, 133–141. DOI:10.1063/1.1774513.

Stone, E. C., & Miner, E. D. (1986). The Voyager 2 encounter with the Uranian system. *Science*, *233*(4759), 39–43. DOI:10.1126/science.233.4759.39.

Strange, N. J., & Longuski, J. M. (2002). Graphical method for gravity-assist trajectory design. *J. Spacecr. Rockets*, *39*(1), 9–16. DOI:10.2514/2.3800.

Tóth, G., Kovács, D., Hansen, K. C., & Gombosi, T. I. (2004). Three-dimensional MHD simulations of the magnetosphere of Uranus. *J. Geophys. Res.*, *109*(A11). DOI:10.1029/2004ja010406.

Turrini, D., Politi, R., Peron, R., Grassi, D., Christina Plainaki, M. B., Lucchesi, D. M., Magni, G., Altieri, F., Valeria Cottini, N. G., Gaulme, P., Schmider, F.-X., Adriani, A., & Piccioni, G. (2013). The ODINUS mission concept – The scientific case for a mission to the ice giant planets with twin spacecraft to unveil the history of our Solar System. White Paper for the Definition of the L2 and L3 Missions in the ESA Science Programme. ArXiv preprint arXiv:1402.2472.

Vasyliunas, V. M. (1986). The convection-dominated magnetosphere of Uranus. *Geophys. Res. Lett.*, *13*(7), 621–623. DOI:10.1029/gl013i007p00621.

Witasse, O., Lebreton, J.-P., Bird, M. K., Dutta-Roy, R., Folkner, W. M., Preston, R. A., Asmar, S. W., Gurvits, L. I., Pogrebenko, S. V., Avruch, I. M., et al. (2006). Overview of the coordinated ground-based observations of Titan during the Huygens mission. *J. Geophys. Res.*, *111*(E7). DOI:10.1029/2005je002640.